



저작자표시-비영리-변경금지 2.0 대한민국

이용자는 아래의 조건을 따르는 경우에 한하여 자유롭게

- 이 저작물을 복제, 배포, 전송, 전시, 공연 및 방송할 수 있습니다.

다음과 같은 조건을 따라야 합니다:



저작자표시. 귀하는 원저작자를 표시하여야 합니다.



비영리. 귀하는 이 저작물을 영리 목적으로 이용할 수 없습니다.



변경금지. 귀하는 이 저작물을 개작, 변형 또는 가공할 수 없습니다.

- 귀하는, 이 저작물의 재이용이나 배포의 경우, 이 저작물에 적용된 이용허락조건을 명확하게 나타내어야 합니다.
- 저작권자로부터 별도의 허가를 받으면 이러한 조건들은 적용되지 않습니다.

저작권법에 따른 이용자의 권리는 위의 내용에 의하여 영향을 받지 않습니다.

이것은 [이용허락규약\(Legal Code\)](#)을 이해하기 쉽게 요약한 것입니다.

[Disclaimer](#)

*Artificial vasa-vasorum as an on-site regenerative
promoter of cell-free vascular grafting*

Hyun-Su Ha

The Graduate School,
Yonsei University
Department of Medicine

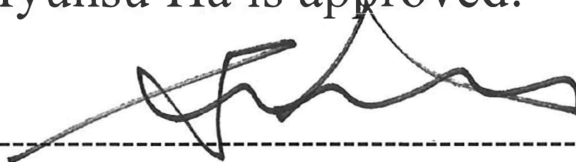
*Artificial vasa-vasorum as an on-site regenerative
promoter of cell-free vascular grafting*

A Dissertation Submitted
to the Department of Medicine
and the Graduate School of Yonsei University
in partial fulfillment of the
requirements for the degree of
Doctor of Philosophy in Medical Science

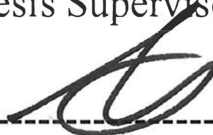
Hyun-Su Ha

June 2024

This certifies that the Doctoral Dissertation of
Hyunsu Ha is approved.



Thesis Supervisor : Hak-Joon Sung



Thesis Committee Member#1 : Jung-Sun Kim



Thesis Committee Member#2 : Chul-Min Ahn



Thesis Committee Member#3: Jayoung Kim



Thesis Committee Member#4: Dae-Hyun Kim

The Graduate School
Yonsei University

December 2023

ACKNOWLEDGEMENTS

In my twenties, I completed a bachelor's degree in chemical engineering and subsequently pursued medical school, ultimately becoming a medical doctor. Following the challenging internal medicine residency program to become specialist, I was fortunate to obtain an incredible opportunity to participate in the MD-PhD program, allowing me to dedicate myself wholeheartedly to scientific research. Reflecting on this academic journey, I have approached the writing of this doctoral thesis with deep introspection and gratitude. As a researcher navigating the intersection of science and clinical medicine, this odyssey has been a continuous exploration of new fields and challenges, providing me with scientific thinking and translational insights that bridge the realms of basic science and clinical practice.

I am humbled and grateful for the guidance and providence of the God that has led me through this process. I extend heartfelt thanks to my beloved wife, Da-hye Son, and my lovely daughter, Jion Ha, for their unwavering support. Above all, I express my deepest gratitude to Professor Hak-joon Sung, my advisor throughout the entirety of my academic journey. His wholehearted support and insightful guidance have been pivotal in shaping the trajectory of this research. I also extend my appreciation to Dr. Kyubae Lee and Sewoom Baek, who shared in the challenges of this research. I am thankful to all the co-authors and lab members who contributed to the collaborative spirit of our research. Special thanks to Professors Jung-Sun Kim, Chul-Min Ahn, Jayoung Kim, and Dae-Hyun Kim for their valuable advice and comments during the thesis writing process. In closing, my gratitude extends to everyone who has played a part in this academic endeavor. This thesis stands as a testament to the collective effort and support that has shaped my academic and professional growth.

TABLE OF CONTENTS

LIST OF FIGURES	iii
ABSTRACT IN ENGLISH	v
1. INTRODUCTION	1
2. MATERIALS AND METHODS	5
2.1. Preparation of cells and animals	5
2.2 Harvest of rabbit arteries	5
2.3. Cell-free scaffold by decellularizing arteries	6
2.4. Quantification of DNA and sulfated(s) GAG	6
2.5. Western blot	7
2.6. Heparin immobilization	8
2.7. <i>In vitro</i> platelet adhesion and activation	8
2.8. Mechanical test	9
2.9. Fabrication of artificial vasa-vasorum	9
2.10. Perfusion and diffusion of AVV	9
2.11. iPSC-EC as an EPC model to recruit by AVV	10
2.12. <i>In vitro</i> macrophage polarization	11
2.13. <i>In vitro</i> EPC migration by macrophage polarization in AVV	11
2.14. <i>In vitro</i> VSMC restoration by macrophage polarization in AVV	12
2.15. ELISA	12
2.16. Arterial grafting models in rabbits	13
2.17. Angiography and doppler sonography	14
2.18. Tissue staining	14
2.19. Quantitative RT-PCR	15
2.20. Data analysis	16
3. RESULTS	17
3.1. Development of Artificial vasa-vasorum. (AVV)	17
3.2. Decellularized vascular scaffold protocol and surface modification.	18
3.3. Heparin immobilization for anti-thrombotic coating.	20
3.4. Artificial vasa-vasorum as a structural and functional vasculature.	21
3.5. <i>In-vivo</i> performance of AVV	22
3.6. “Inside-out” and “Outside-in” re-endothelialization of cell-free scaffold.	25

3.7. <i>In vivo</i> Macrophage M2 polarization by AVV	27
3.8. <i>In vitro</i> macrophage phenotypic modulation by microchannel network	28
3.9. In-vitro EPC migration assay	29
3.10. VSMC restoration and vascular remodeling after day 30 post-implantation.	30
3.11. <i>In vitro</i> VSMC differentiation from hMSC promoted by microchannel network.	32
3.12. Regenerated elasticity of cell-free scaffold by VSMC restoration.	33
3.13. Versatile utility of AVV	34
4. DISCUSSION	37
5. CONCLUSION	39
REFERENCES	40
ABSTRACT(IN KOREAN)	43

LIST OF FIGURES

<Fig 1> Concept of artificial vasa-vasorum (AVV) .	3
<Fig 2> PNIPAM fiber mimicking structural function of capillary vessel.	18
<Fig 3> Fabrication step and gross appearance of artificial vasa-vasorum with cell-free scaffold.	19
<Fig 4> Investigation of Decellularization Methods for Vascular Scaffolds and characterization.	21
<Fig 5> Effect on radial tensile strength of vascular scaffold by decellularization protocols.	22
<Fig 6> Anti-thrombosis effect of heparin immobilization.	23
<Fig 7> AVV Promote perfusion and diffusion capacity and EC tube formation.	24
<Fig 8> Schematic illustration of animal study.	25
<Fig 9> Gross appearance of day 14 post operation and angiography images of rabbit carotid interposition model.	25
<Fig 10> Histological analysis and blood flow data for AVV in rabbit carotid artery interposition model.	27
<Fig 11> Schematic illustration of inside-out and outside-in re-endothelialization.	28
<Fig 12> Histology and immunostaining result validate re-endothelialization capability of AVV.	29
<Fig 13> Angiogenic potential of AVV recruit EC and EPC to cell-free scaffold.	30
<Fig 14> <i>In vivo</i> macrophage phenotype modulation effect of AVV.	31
<Fig 15> Microchannel network promote M2 macrophage polarization.	32
<Fig 16>. Radius EPC migration assay demonstrate the mechanism of early re-endothelialization	33
<Fig 17> VSMC restoration and vascular remodeling at day 30 post-implantation.	34
<Fig 18> Comparing protein and gene expression level of VSMC restoration.	34
<Fig 19> VSMC differentiation from MSC was promoted by TGF- β signaling of M2 macrophage.	35
<Fig 20> <i>In vitro</i> trans-well study for elucidating the mechanism of VSMC restoration.	36
<Fig 21> <i>Ex-vivo</i> tensile test to investigate VSMC restoration.	37
<Fig 21> Rabbit femoral artery model for end-to-end anastomosis of very small artery ($\leq 1\text{mm}$).	38
<Fig 22> Effects of AVV on $\leq 1\text{mm}$ sized vascular grafting models: Histological and Functional Analysis	39
<Fig 23> Effects of AVV on end-to-side anastomosis grafting model.	39

ABSTRACT

Artificial vasa-vasorum as an on-site regenerative promoter of cell-free vascular grafting

The small-diameter artificial vessels as an alternative to autologous vascular graft still have challenges in clinical application due to issues such as thrombosis, neointima, and most significantly, the poor cellular regeneration of the scaffolds after grafting. Here we report the development and preclinical therapeutic efficacy of an artificial vasa vasorum (AVV), which facilitates cell recruitment around a cell-free scaffold and promotes re-endothelialization and vascular smooth muscle regeneration. The graft consists of a gelatin hydrogel-based 3D microchannel network, fabricated through the utilization of temperature-responsive polymer with micro-spinning technique, and a cell-free artery scaffold designed to minimize mechanical property loss. In rabbit carotid artery interposition model, the artificial vasa-vasorum enhanced the re-endothelialization and angiogenesis through endothelial progenitor cell (EPC) recruitment and M2 macrophage polarization. Additionally, the cellular recruitment and inflammation modulation effect of AVV significantly foster smooth muscle regeneration, leading to improved vascular elasticity restoration and increased long-term patency. The "Outside-in" strategy, as regenerator of vascular scaffold, offers a promising novel approach to address unmet clinical needs effectively.

Key words : Microchannel network, artificial artery, cell-free, endothelialization, tissue-engineered vascular graft

I. INTRODUCTION

Cardiovascular diseases resulting from the narrowing or blockage of small-diameter blood vessels (< 6 millimeters) are a leading cause of death worldwide.¹ In patients with severe coronary artery disease or peripheral arterial disease, vascular grafts are utilized to replace or bypass damaged blood vessels. In the United States alone, approximately 400,000 coronary artery bypass graft (CABG) procedures are performed annually². However, the harvesting process of autologous vessels is not only invasive but also reported that over 30% of cardiovascular disease (CVD) patients do not have suitable autologous vessels available for grafting³. Furthermore, when saphenous vein grafts are used for CABG surgery, graft failure occurs in approximately 10-20% of cases within one year due to thrombosis and neointimal hyperplasia. Additionally, vein grafts present challenges in performing interventional procedures like stent insertion when the stenosis occurs, and it is difficult to secure additional autologous vessels for reoperation⁴. The necessity for developing artificial small-diameter vascularE grafts has been recognized, and tissue-engineered vascular grafts (TEVG) using biocompatible materials with tailored physical properties have emerged as a promising solution to address these challenges.

Numerous researchers have attempted to fabricate tissue-engineered vascular grafts (TEVGs) using cell-based approaches. Since the first report of TEVG in 1986, where bovine endothelial cells(ECs), fibroblasts, and smooth muscle cells(SMCs) were cultured on a collagen matrix, significant advancements have been made in developing various cell-based graft fabrication methods utilizing bioreactors and 3D culture systems.^{5,6} Clinical translation of cell-based grafts for TEVG fabrication has been hindered by challenges such as lengthy cell isolation and in vitro culture, low cellular proliferation rates, difficulties in obtaining patient-derived cells and standardization, high costs, and cell contamination issues.^{7,8} Due to these limitations of cell-based TEVGs, there has been an increasing demand for the use of functionalized cell-free scaffolds⁹.

Decellularized vascular scaffolds are a promising biomedical material that retains the native extracellular matrix components and structure of vascular tissues, such as collagen, elastin, and glycosaminoglycan (GAG), while eliminating cellular elements and antigenicity¹⁰. However, overcoming the poor recellularization capacity of dense extracellular matrices lacking cellular components remains a challenge to be addressed in decellularized vascular scaffolds. The

insufficient recellularization capability leads to restricted re-endothelialization within the vascular lumen, resulting in exposed collagen and basement membrane that trigger activation of circulating platelets and the extrinsic coagulation cascade, leading to thrombus formation and subsequent obstruction¹¹. Furthermore, the poor cell infiltration within the vascular scaffold leads to inadequate vascular remodeling, causing neointimal hyperplasia and stenosis¹².

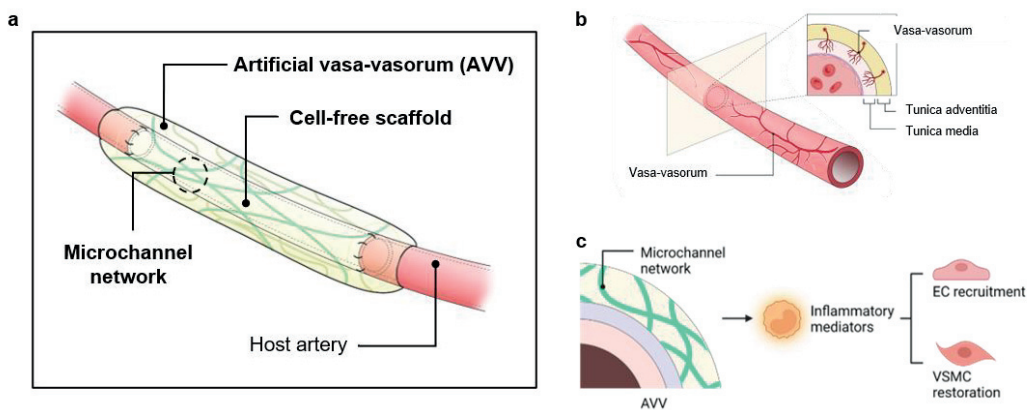


Figure 1. Concept of artificial vasa-vasorum (AVV)

To address this problem, we developed a novel hydrogel-based 3D microchannel network system, mimicking the vasa vasorum structure, to re-endothelialize the vascular lumen and facilitate recellularization of cell-free vascular scaffolds (**Figure. 1a**).

Vasa vasorum is a Latin term that means "vessels of vessels," and it refers to a unique vascular network that supplies blood, oxygen, and nutrients to the cells composing the walls of larger blood vessels (**Figure 1b**)¹³. The "no touch technique," which preserves the vasa vasorum during surgery, is widely accepted in coronary artery bypass surgery patients for promoting endothelial progenitor cell (EPC) recruitment and enhancing vein graft patency¹⁴. In contrast, TEVG research has predominantly focused on the physical, chemical, and surface properties of the scaffold over the past few decades, while the regenerative role of vasa-vasorum in the graft has been overlooked. Meanwhile, the emergence of the "Outside-in theory" has highlighted the critical role of perivascular cells in inflammation cascade and pathophysiology during early atherosclerosis and plaque formation processes¹⁵. Based on this background, our study aims to propose a novel

outside-in regenerative strategy for vascular scaffolds by utilizing AVV through tissue-engineering technology.

Cell-free artery scaffolds require rapid luminal endothelialization to prevent early thrombosis-induced obstruction. While surface coating techniques such as Fibronectin, Heparin, Biomimetic peptides, and others have been proposed as solutions for thrombosis prevention, they have not yielded satisfactory results in clinical application. Therefore, additional approaches are needed to effectively promote the recruitment of vascular endothelial cells¹⁶. A lot of reports have identified circulating endothelial progenitor cells (EPCs) and monocytes as the key players responsible for luminal endothelialization of grafts¹⁷. These circulating cells undergo repopulation within the lumen (known as "Fallout endothelialization") by being induced homing, migration, and mobilization through angiogenesis signals triggered by inflammation following vascular injury^{18,19}. For a cell-free vascular graft to achieve long-term patency, successful regenerative responses and remodeling processes in the media and adventitia layers are important, following the luminal endothelialization. In order to facilitate successful vascular graft remodeling, sufficient monocyte infiltration is necessary in early phase, and during this process, it is crucial to prevent prolonged M1 pro-inflammatory macrophage activation and induce M2 anti-inflammatory macrophage polarization to promote EPC recruitment and endothelial cell proliferation²⁰. Furthermore, M2a macrophages, identified by the expression of ARG-1 as a biomarker, are known to promote vascular graft remodeling and endothelial cell stabilization through IL-4, IL-10, and TGF- β signaling²¹. Additionally, TGF- β signaling has been shown to induce the differentiation of mesenchymal progenitor cells into mature vascular smooth muscle cells (VSMCs)²². VSMCs significantly contribute not only to the formation of hemodynamically laminar blood flow through promoting elasticity of vessel and contractile function but also increase long-term patency by participating in EC-VSMC crosstalk and processes related to extracellular matrix (ECM) synthesis and degradation²³. Indeed, M2 macrophage immunomodulation, leading to early luminal re-endothelialization and long-term VSMC restoration, is essential for small-diameter vascular grafting using TEVG.

Recently, we reported the successful implementation of a dense microchannel network using temperature-responsive polymer Poly(N-isopropylacrylamide) (PNIPAM) as sacrificial fibers within gelatin-based hydrogel. Through this approach, we were able to promote angiogenesis and

regeneration at ischemic injury sites.²⁴. The fabricated functional vascular structure within the hydrogel effectively enhanced the diffusion capacity of oxygen and nutrients within the body, and it successfully promoted proangiogenic M2 polarization of macrophages²⁵. Based on this technical background, we hypothesized that the artificial vascular vessel (AVV) would polarize macrophages as inflammation mediator into M2 phenotype, and through this process, it would induce endothelial cell (EC) recruitment and vascular smooth muscle cell (VSMC) restoration **(Figure 1c)**.

This study aims to propose a novel vascular grafting strategy by integrating decellularized vascular scaffold with heparin immobilization and microchannel network-containing functional artificial vasa vasorum. And we aimed to investigate the cellular regenerative effects of the AVV. The rabbit carotid interposition model, as the end-to-end anastomosis model of 1-2 mm sized small-diameter blood vessels, demonstrated the inside-out and outside-in endothelialization effects mediated by M2 macrophages in early phase (1-2 weeks post-implantation), followed by VSMC remodeling and its restoration mechanism in late phase (> 4 weeks after implantation). Additionally, the femoral artery interposition model as tiny vessel model (diameter < 1 mm) showed the effectiveness of the AVV. Also, aorta-to-iliac grafting with the end-to-side anastomosis model evidence various utility and versatility of AVV.

2. MATERIALS AND METHODS

2.1. Preparation of cells and animals

Raw 264.7 cell (ATCC, Manassas, VA, USA), human endothelial progenitor cell (EPC; Cellprogen, Benelux, Netherlands), human mesenchymal cell (hMSC; Lonza, Basel, Switzerland) were purchased with no ethical issues. Raw 264.7 cells were cultured using Dulbecco's Modified Eagle's Medium-High glucose (DMEM; Gibco, Carlsbad, CA, USA) supplied with 10% fetal bovine serum (FBS; 16000-044, Gibco) and 1% penicillin-streptomycin (PS; 15140-122, Gibco). hMSCs were culture using Dulbecco's Modified Eagle's Medium-Low glucose (Gibco). EPCs were cultured using progenitor cell complete media with serum (M36081-13S, Celprogen, Torrance, CA, USA) following the manufacturer's manual. Each cell type was propagated until 80% confluency and detached using 0.25% trypsin/ethylenediaminetetraacetic acid (Trypsin/EDTA; Gibco) for subculture.

Human induced pluripotent stem cells were reprogrammed to endothelial cells (hiPSC-EC) following the previous report²⁶ and cultured in mTeSR 1 medium (85850, STEMCELL Technologies, Vancouver, Canada) on 5% Matrigel (354277, Corning, NY, USA)-coated plates at 37 °C with 5 % CO₂. The medium was exchanged every day until reaching 95% cell confluency in a 100 mm dish, followed by detaching hiPSC-ECs with Phosphate Buffered Saline (PBS; 1X, Welgene, Gyeongsangbuk-do, Republic of Korea) containing 0.5 mM EDTA. Then, the cells were transferred to an anti-attached tube using mTeSR 1 medium and 5% Matrigel, which was coated onto an ultra-low attachment 100 mm petri dish. The culture medium containing 5 % Matrigel was changed every day for 3 days on a shaker at 37 °C with 5 % CO₂. After enzymatically dissociating, clumps of hiPSCs (passages < 60) were differentiated to ECs by culturing on 0.01 % collagen-coated plates in DMEM/F12 medium supplemented with 20 % serum replacement with specific differentiation factors for 10 days. The rabbit study was approved by the Institutional Animal Care and Use Committee of Yonsei University College of Medicine (2021-0048 for rabbit experiments). All rabbit (3kg, male, New Zealand White) were purchased from Doo Yeol Biotech (Seoul, Republic of Korea).

2.2. Harvest of rabbit arteries

The rabbit study was approved by the Institutional Animal Care and Use Committee of Yonsei University College of Medicine (2021-0048 for rabbit experiments). Rabbits (3 kg, male, New Zealand White) were purchased from Doo Yeol Biotech (Seoul, Republic of Korea). All animals were acclimated to an animal facility for a minimum of one week prior to surgery. Each rabbit was anesthetized through intramuscular injection of zoletil (50 mg kg⁻¹, Zoletil™, Virbac Korea, Seoul, Republic of Korea) and xylazine (5 mg kg⁻¹, Rompun®, Bayer Korea, Seoul, Republic of Korea), followed by euthanasia via intravenous injection of potassium chloride (20 mg kg⁻¹; Choongwae Pharma Corporation, Seoul, Republic of Korea). For the purpose of in vitro test and carotid artery interposition surgery, rabbit carotid artery allografts were harvested. After a midline incision was made into the neck skin, carotid artery branches were ligated using 9-0 sutures (Ethicon, Raritan, NJ, USA), followed by cross-clamping on the proximal and distal sides of artery. A 5 cm segment of carotid artery was excised and gently washed with sterilized PBS to remove intravascular thrombus for storage at 4 °C. Likewise, for femoral artery interposition surgery, femoral artery allografts were obtained, and for the aorta to iliac artery bypass surgery, aorta allografts were harvested from euthanized rabbits.

2.3. Cell-free scaffold by decellularizing arteries

The harvested arteries were decellularized by either mechanochemical [freeze-thaw cycling with 1 % Triton X-100 (93443, Sigma-Aldrich, St. Louis, MO, USA)] or chemicochemical [1% sodium dodecyl sulfate (SDS; L3771, Sigma-Aldrich) with 1% Triton X-100 (Sigma-Aldrich)] method. Briefly, the mechanochemical method was proceeded by freezing and thawing the artery at -80 °C and 37 °C for 30 min, respectively with repetitions for 10 times, followed by treatment with 1 % Triton X-100 at 37 °C for 30 min. In contrast, the chemicochemical process was carried out by treating the artery with 1% SDS for 48 h and then with 1% Triton X-100 at 37 °C for 12 h. The decellularized arteries were defined as cell-free scaffolds; washed with double-distilled water; and sterilized by treating with 0.4 % peracetic acid (Sigma-Aldrich) and 70% EtOH (Sigma-Aldrich) for 30 min each, followed by PBS washing and lyophilizing (7960041, Labconco, KS, USA).

2.4. Quantification of DNA and sulfated(s) GAG

Both native and decellularized arteries were washed twice with PBS, freeze-dried, and digested by papain solution (Sigma-Aldrich) at 60 °C for 6 h. The lysates were used to determine the amounts of double-stranded DNA (dsDNA) content using the Quant-iT PicoGreen dsDNA assay kit (ThermoFisher, MA, USA). The lysate samples were mixed with the Quant-iT PicoGreen reagent, which were subjected to fluorescence reading at 480 nm (excitation) and 520 nm (emission) using a fluorescence microplate reader (Varioskan Flash 3001, ThermoFisher, MA, USA). The sGAG content of each lysate was quantified by a Blyscan™ Glycosaminoglycan Assay Kit (Biocolor, County Antrim, UK) according to the manufacturer's instruction. Briefly, 1,9-dimethylmethylene blue cationic dye was reacted with the sulfated sGAG in the lysate solution, which was centrifuged for 30 minutes at 14,000 rpm and resuspended using a dye dissociated buffer. Then, the absorbance was measured at 656 nm in a microplate reader.

2.5. Western blot

After storing in PBS at -20 °C, the artery samples were minced using scissors and tissue homogenizer (Tissuruptor II, QIAGEN, Hilden, Germany) in RIPA buffer (R0278, ThermoFisher) with 1x protease inhibitor (78833, ThermoFisher). The protein content of each lysate was quantified using the Bradford assay (B6916, Sigma-Aldrich). Then western blotting was carried out to analyze the expression of vascular proteins. Gel electrophoresis was performed using 10% SDS-polyacrylamide gels (10% w/v, 4561094, Bio-Rad, USA), and the proteins were transferred onto a nitrocellulose membrane (IB23001, ThermoFisher). The membrane was then blocked with 5% nonfat dry milk (1706404, Bio-rad, USA) in tris-buffered saline with 0.5% Tween-20 (TBST, BTT-9110, Tech & Innovation, Kangwon-do, Republic of Korea) and incubated with target primary antibodies for 24h at 4°C. After washing step, the membrane was reacted with secondary antibodies conjugated to HRP. Primary antibodies included β -actin (1:200, SC-47778, Santa Cruz Biotechnology, Dallas, TX, USA), CD31 (1:100, NB600-562, Novus Biologicals LLC, Centennial, CO, USA), α SMA (1:100, Invitrogen, Carlsbad, CA, USA), and Type 1 collagen (1:1000, NB600-408, Novus Biologicals LLC). Secondary antibodies included goat anti-rabbit antibody (1:1000, 31460, ThermoFisher) and goat anti-mouse antibody (1:1000, 31430, ThermoFisher). Chemiluminescence signals were visualized using an ECL substrate (1705060, Bio-rad), and the signals were captured using a

gel documentation system (ImageQuant LAS 4000, GE Healthcare Life Sciences, Chicago, IL, USA).

2.6. Heparin immobilization

Heparin was immobilized onto the cell-free scaffolds through reaction of 1-ethyl-3-(3-dimethylaminopropyl) carbodiimide (EDC) and N-hydroxysuccinimide (NHS) (both from Sigma-Aldrich, St. Louis, MO, USA). Briefly, heparin (2000 I.U., JW Pharmaceutical Corporation, Seoul, Republic of Korea), EDC (120 mmol/L), and NHS (60 mmol/L) were reacted in 2-(N-morpholino) ethanesulfonic acid (MES; 0.1M, pH 6.0, Biosolution, Seoul, Republic of Korea) buffer for 30 min at room temperature to activate carboxylic acid groups of heparin. The pH of solution was adjusted to 8-9 using NaOH (Duksan, Gyeonggi-do, Republic of Korea), followed scaffold immersion for 4 h at room temperature with continuous shaking. After washing with double-distilled (DI) water, the amount of immobilized heparin in each scaffold was determined by staining with Toluidine blue O solution (1 mL, Sigma-Aldrich) containing 0.1 M HCl at room temperature for 4 h, followed by DI water washing for 24 h to remove residual TBO solution. Then, the samples were dissolved in a mixture of 0.1 M NaOH and ethanol (1:4, volume ratio) until complete decolorization and subjected to absorbance reading at 530 nm in a microreader. Mechanical test

2.7. *In vitro* platelet adhesion and activation

The heparin immobilization was verified by testing platelet adhesion and activation on the scaffolds. Fresh platelets were extracted from the whole blood of New Zealand white rabbits (male, 6 months old, weight: 2.0-2.5 kg) whole blood, following the guidelines of Yonsei Laboratory Animal Research Center. The scaffolds (+/- heparin immobilization) was reacted with platelets in PBS dilution at 37 °C for 1 h, followed by twice PBS washing, fixing with 2 % glutaraldehyde in PBS for 6 h, and dehydration using a Critical Point Dryer (EM CPD300, Leica, Austria). The adhesion and activation of platelets on the test scaffolds were visualized using a scanning electron microscope (SEM, MERLIN, Zeiss Merlin, Oberkochen, BW, Germany) with quantitative image analyses.

2.8. Mechanical test

Circumferential tensile properties of vessel samples were characterized to analyze i) changes in the mechanical properties through the decellularization processes and ii) the elasticity restoration by smooth muscle regeneration after 1 month-implantation. The tubular samples were vertically sectioned and flattened within 1 h post-surgery to minimize alterations of tissue characteristics. After cutting each flattened sample in the circumferential direction into the uniform size (width x length: 5 x 7 mm), the tensile strength and Young's modulus were measured by DMA (DMA 850, TA instrument Inc. New Castle, DE, USA) under 10 % min⁻¹ of the strain rate at 37 °C.

2.9. Fabrication of artificial vasa-vasorum (AVV)

A custom-build mold was created using polydimethylsiloxane (PDMS; Dow Corning, Midland, MI, USA) with the dimension of 3 (width) × 5 (depth) × 1 (height) cm, and a tubular space with the size of 6 (diameter) mm × 4 (length) cm was obtained by casting a cylinder with curing. A silicone tube with the artery size of 2 (diameter) mm × 5 (length) cm was placed in the center of cylinder space inside the mold. As a thermo-sensitive polymer, poly(N-isopropylacrylamide) (PNIPAM, Mw = ~40,000, Sigma–Aldrich, St. Louis, MO) was used to produce a thread of sacrificial fibers as the means to generate a channel network. The PNIPAMA powder was dissolved in methanol (53 % w/v), which was subjected to fiber spinning at 2500-2800 rpm using a customized device as reported previously^{25,27}. A tread of microfibers in 20-30 μm diameter was obtained and evenly placed around the silicone tube in the cylinder space of PDMS mold. Then, gelatin and microbial transglutaminase (mTG) were mixed (9:1 ratio) in a PBS (5% w/v), which was poured into the cylinder space to cover the fibers and silicone tube, followed by mTG crosslinking reaction at 37 °C. Next, the PNIPAM microfibers were dissolved from mTG hydrogel through sol-gel transition by immersing and perfusing with cold PBS (4 °C), thereby generating a channel network in the mTG gel as a form of AVV upon replacement of silicone tube with a cell-free scaffold.

2.10. Perfusion and diffusion by AVV

The microchannel network of gel was stained by perfusing microbead (0.1 μm, Invitrogen) first.

As key functions of microvessel network, AVV was then tested by perfusing microbeads (2 μm , Invitrogen) and diffusing Fluorescein Isothiocyanate (FITC)-dextran (FITC-dextran; 40 kDa, Sigma-Aldrich). As in vitro samples, gels (+/- microchannel network) were prepared with embedding silicone tube (Inner diameter = 1 mm, outer diameter = 2 mm; SL-0102, LK LAB Korea, Gyeonggi-do, Republic of Korea) as a model of cell-free scaffold. The silicone tube was connected by a straight connector (30622-49, SCIST, Donginbio, Seoul, Republic of Korea). As in vivo samples, the grafts were harvested at day 30 post implantation into a rabbit carotid artery through interposition surgery. A straight connector was attached to the scaffold using 4-0 silk suture (Ethicon) for a leak-free connection. Then, a syringe pump (LEGATO210, KdScientific, Holliston, MA, USA) was used to perfuse red microbeads (1:5000 in PBS) at a rate of 20 $\mu\text{L min}^{-1}$ or FITC-dextran (0.1 w/v % in PBS) was diffused into the gels through an inlet connector under confocal imaging (LSM 980, Zeiss, Oberkochen, Land Baden-Württemberg, Germany). Colormaps were visualized using ImageJ software, followed by quantitative analysis using MATLAB software (Mathworks, USA) (N = 4, each group).

2.11. iPSC-EC as an EPC model to recruit by AVV

As an EPC model, iPSC-ECs were embedded into the gelatin/mTG solution (1×10^7 cells mL⁻¹), which was used to produce the graft samples with AVV or (-) channel. These samples were exposed to a closed circulation of culture media upon perfusing into the inlet silicone tube in connection with the graft samples so that iPSC responses to the perfusion and diffusion of media by the channel network could be examined. An arterial flow was generated at a continuous rate of 346.9 $\mu\text{L min}^{-1}$ using a peristaltic pump (BT100-1L-A, Baoding Longer Precision Pump, Hebei, China) for 7 days. The graft samples were fixed in 4% paraformaldehyde at 4 °C for 1 day with thrice PBS washing, followed by cell permeabilization using 0.3 % Triton X-100 in PBS at room temperature for 1 h with thrice PBS washing. Cell viability was then determined using the Live/DEAD Viability/Cytotoxicity Kit (L3324, Invitrogen) by incubating samples with 4 mM calcein-AM (live-green) and 2 mM ethidium homodimer-1 (dead-red) for 30 min in the culture media. After counter staining of nuclei with DAPI (R37606, ThermoFisher) at room temperature for 20 min, the samples were subjected to confocal imaging (LSM 980, Zeiss) with qualitative and quantitative image analyses of viable endothelialization into the samples.

2.12. *In vitro* macrophage polarization

Gel samples (5 w/v % +/- channel network) were prepared in a disc size of 1 cm (diameter) x 2 mm (thickness) (N = 4 each group). Raw 264.7 macrophages (ATCC, 1×10^6 cells) were cultured onto each hydrogel sample in High-glucose DMEM medium for 2 days. Then, macrophages were activated by treating with $1 \mu\text{g mL}^{-1}$ of lipopolysaccharide (LPS; Sigma-Aldrich) for 7 days, followed by fixing with 4% paraformaldehyde (CellNest) for 24 h. The samples were permeabilized with 0.1% Triton X-100 (Sigma-Aldrich) in PBS and blocked with 5% bovine serum albumin (BSA; 82-100-6, Millipore, Burlington, MA, USA) at room temperature for 2 h. Macrophage polarization was determined by immunofluorescent staining with sample treatment using primary antibodies against ARG-1 (M2 marker, 1:100, NBP1-43347, Novus) and iNOS (M1 marker, 1:100, GTX17504, Genetax, Irvine, CA, USA) overnight at 4 °C. The samples were washed and incubated with secondary antibodies for 2 h in the dark, followed by nucleus counterstaining with NucBlue Live Ready Probes Reagent (Invitrogen) and confocal imaging (LSM 780, Zeiss) with quantitative analysis.

2.13. *In vitro* EPC migration by macrophage polarization in AVV

Raw 264.7 cells (ATCC, 1×10^6 cells mL⁻¹) were embedded into gelatin hydrogels (0.5 cm diameter and 2 mm thickness +/- channel network) as described above and cultured in high glucose DMEM media (Gibco) for 3 days (N = 4, each group). Then, LPS ($1 \mu\text{L min}^{-1}$) was treated to activate macrophages (day 0) and used to determine EPC migration by M2 polarization of macrophages due to the microchannel effect. Following the manufacturer's instruction, the radius migration assay (CBA-125, Cell Biolabs, San Diego, CA, USA) was carried out by seeding EPCs (2×10^5 cells per well) in specialized 24-well plates (112501, Cell Biolabs) whose center (diameter 0.68 mm) was coated with a biocompatible radius gel. After culturing EPCs for 24 h, the central gel was removed using a gel removal solution (112504, Cell Biolabs), thereby generating a cell-free circular region. Then, the gel samples with activated macrophages were placed on the cell-free region and subjected to 14 day-culture, followed by determining EPC migration towards the cell-free region. After removing the hydrogel samples, EPCs were fixed with 4 % paraformaldehyde (CellNest) for 24 h and treated using Alexa488-labeled F-actin (A12379, Thermofisher). Subsequently, the imaging studies

utilizing confocal microscopy (LSM 780, Zeiss) were performed after PBS washing and nucleus staining steps.

2.14. In vitro VSMC restoration by macrophage polarization in AVV

Because AVV was proposed to induce M2 polarization of macrophages with TGF- β production, mesenchymal stem cells (hMSCs, Lonza, Switzerland) were used as a precursor cell type of VSMCs to determine the direction of differentiation by qRT-PCR and immunostaining. Gel samples (+/- channel network) with a disc size of 1 cm (diameter) \times 2 mm (thickness) were prepared. Raw 264.7 macrophages were seeded onto the gel samples in a 6-well culture plate (1×10^6 cells mL⁻¹) and cultured for 48 h. Then, the samples were treated with LPS (1 μ g mL⁻¹, Sigma-Aldrich) for macrophage activation and placed in the top chamber of trans-well plate (35006, SPL, Pore size 0.4 μ m, Gyeonggi-do, Republic of Korea), followed by seeding hMSCs (5×10^5) onto the bottom chamber to co-culture for 7 days. The amount of TGF- β was determined using ELISA by obtaining the supernatant from the upper chamber media. The samples were fixed with fixing with 4% paraformaldehyde, permeabilized with 0.25 % Triton X-100 solution (Thermofisher), blocked, washed, and incubated with the primary antibody (α SMA; 1:1000, Abcam) at 4 °C for 24 h with PBS washing. The fluorescent-labeled secondary antibody (A28175, Alexa Fluor 488 Goat anti-Mouse; 1:1000, Thermofisher) was then treated to the samples for 2 h at room temperature, followed by confocal imaging (LSM 780, Zeiss).

2.15. ELISA

The TGF- β ELISA kit (Thermofisher) was used following the manufacturer's instruction. A 96-well plate (9018, Corning, USA) was coated with the capture antibodies by incubating overnight at 4 °C, which was blocked with diluent at room temperature for 1 h. Recombinant TGF- β was used to generate a standard curve through 2-fold serial dilutions to reach 8 points. Latent TGF- β was converted into an immunoreactive form through acid activation by treating with 1N HCl, followed by neutralization with 1N NaOH. The co-culture supernatant (100 μ L) and blank control were added to the wells with sealing and incubated at room temperature for 2 h or overnight at 4 °C to increase the sensitivity. Next, the detection antibodies were added

to the wells and incubated at room temperature for 1 h, followed by incubating with Avidin-HRP at room temperature for 30 min. The fluorescence intensity was measured at 450 nm by subtracting the background value (570 nm) in a microplate reader.

2.16. Arterial grafting models in rabbits

All procedures were approved by the Institutional Animal Care and Use Committee (IACUC) of Yonsei University College of Medicine as denoted above. Male rabbits (3 kg) underwent a one-week acclimation period before the surgeries. To prevent thrombosis on the grafts upon implantation, aspirin (5mg kg⁻¹, Bayer, Leverkusen, Germany) was administered orally into each rabbit from day 3 before surgery until day 14 post-surgery. Each rabbit was anesthetized through subcutaneous injection of zoletil (10 mg kg⁻¹, Virbac, Seoul, Republic of Korea), which was maintained via endotracheal inhalation of isoflurane (2 - 2.5%, Hana Pharm, Gyeonggi, Republic of Korea).

As a model of central small artery (1-1.5 mm in diameter), a carotid artery of each rabbit was subjected to surgical interposition with the graft (AVV + cell-free scaffold) by starting to make a 4 cm incision at the center anterior neck so that the carotid artery was exposed through dissection of the subcutaneous tissue and neck muscle. The branches of carotid artery were tied to block blood flow using 9-0 ethilon sutures (Ethicon), followed by intravenous injection of heparin (100 IU kg⁻¹, JW Pharmaceutical, Seoul, Republic of Korea). Then, both proximal and distal sides of artery were clamped using micro devices (JD-S-101MC, Jeung Do Bio, Seoul, Republic of Korea), and the arterial segment between the clamps was excised. The graft (2 cm in length) was inserted into the segment spot with end-to-end anastomosis using a 9-0 ethilon suture (Ethicon), and the neck soft-tissue was closed using 4-0 vicryl suture (Ethicon), followed by skin closure using 4-0 ethilon suture (Ethicon). Secondly, the femoral artery interposition procedures (using a \leq 1mm diameter caliber artery model) were performed as follows. Initially, a 4 cm linear incision was made on the right hind limb to access the tissue and expose the femoral artery. Subsequently, similar to the carotid artery interposition procedure, the proximal and distal arteries were clamped and excised, followed by an end-to-end anastomosis of a 2cm-sized decellularized femoral artery. Lastly, the graft was bypassed from aorta to iliac artery graft by starting to make a linear incision (7-8 cm) along the mid-line of the abdomen so that the abdominal cavity was exposed by dissecting the muscles and fascia. Gauzes were soaked

in warm saline and placed in the cavity to prevent hypothermic injury and tissue dehydration while surgery. Next, the retroperitoneal space around the aorta bifurcates and the iliac arteries were identified by careful dissection. In this procedure, 3cm sized decellularized aorta graft with AVV were used to grafting. Then, the proximal aorta and the distal side of the right and left iliac arteries were clamped, followed by bypass grafting through end-to-side anastomosis with the aorta and through end-to-end anastomosis with the iliac artery using 9-0 Ethilon sutures (Ethicon). Soft tissues and then skin was closed using a 4-0 vicryl and 4-0 ethilon suture (Ethicon), respectively.

After the surgeries, rabbits were carefully monitored daily for 30 days under pain control by administering meloxicam (0.5 mg kg^{-1} , Medica Korea, Seoul, Republic of Korea) once a day orally for the first 7 days. Infection was prevented by administering orally enrofloxacin (10 mg kg^{-1} , CTBio Inc. Hwaseong-si, Gyeonggi-do, Republic of Korea) for the first 7 days. The rabbits were euthanized using a bolus intravenous injection of potassium chloride (20 mg kg^{-1} ; Choongwae Pharma Corporation) under general anesthesia, followed by harvesting tissue samples at the surgical sites for analyses.

2.17. Angiography and doppler sonography

Ultrasonography (iU22 xMatrix DS, Philips, Amsterdam, Netherlands) was carried out to examine blood flow profiles on day(s) 0 (right after grafting), 7, 14, and 30 ($N = 5$ for each group). The blood flow was analyzed by making color doppler and PW (Pulse Wave) modes. Angiography was performed to the carotid and femoral arteries (day 30) and the bypass graft (day 14) using a C-arm x-ray equipment (General Electric, NY, USA). The femoral artery (non-surgical site) was exposed by making an incision and dissecting the subcutaneous tissues and muscles, followed by inserting a 4 Fr sheath (TERUMO, Seoul, Korea) into the artery. Next, a 0.014-inch guidewire (Asahi Intecc Medical, Tokyo, Japan) was introduced through the to the target site with positioning a 4 Fr catheter (Glidecath®, TERUMO) near the target site following the guidewire path. Contrast media (Scalnox, SANOCHEMIA, Austria) was mixed with normal saline (1:1 ratio, Choongwae Pharma Corporation), which was then injected into the catheter to acquire vessel images.

2.18. Tissue staining

After harvesting, grafts were embedded in paraffin, cross-sectioned into 5 μm slices, and H&E stained. For immunofluorescence staining, tissue sections were deparaffinized using xylene (Duksan) and rehydrated in ethanol (Duksan) through a series of incubations (100%, 95%, 80%, 70% (v/v) in distilled water). Antigen retrieval was achieved by heating slides in citrate buffer (1X, pH 6.0, Sigma-Aldrich) at 95 °C for 30 minutes. Subsequently, endogenous peroxidases were inactivated with 3% H₂O₂ solution for 10 minutes. Tissue sections were permeabilized using 0.1% Triton X-100 for 1h and blocked with 5% BSA (Millipore) in TBST at room temperature for 2 h. Samples were treated with primary antibodies against CD31(1:100, NB600-562, Novus), CD11b (1:100, Ls-B3760, LS Bio, Seattle, WA, USA), α -SMA (1:100, NB300-678, Novus), ARG-1 (1:200, LS-C447907, LS Bio), and/or iNOS (1:200, GTX17504, Genetex), MYH-11 (1:200, NBP2-44532, Novus) overnight at 4 °C. After thrice PBS washing, samples were incubated with secondary antibodies including anti-rabbit Alexa Fluor 488 and 594 (1:1000, 111-545-003 and 11A1-585-003, Jackson ImmunoResearch Laboratories), anti-goat Alexa Fluor 488 (1:1000, A11055, Invitrogen), and/or anti-mouse Alexa Fluor 594 (1:1000, A11005, Invitrogen) for 2 h in the dark. After 3 times PBS washing for 10 minutes each, confocal imaging (LSM 780, Zeiss) was conducted after nucleus staining.

2.19. Quantitative RT-PCR

After harvesting, grafts were embedded in paraffin, cross-sectioned into 5 μm slices, and H&E stained. For immunofluorescence staining, tissue sections were deparaffinized using xylene (Duksan) and rehydrated in ethanol (Duksan) through a series of incubations (100%, 95%, 80%, 70% (v/v) in distilled water). Antigen retrieval was achieved by heating slides in citrate buffer (1X, pH 6.0, Sigma-Aldrich) at 95 °C for 30 minutes. Subsequently, endogenous peroxidases were inactivated with 3% H₂O₂ solution for 10 minutes. Tissue sections were permeabilized using 0.1% Triton X-100 for 1h and blocked with 5% BSA (Millipore) in TBST at room temperature for 2 h. Samples were treated with primary antibodies against CD31(1:100, NB600-562, Novus), CD11b (1:100, Ls-B3760, LS Bio, Seattle, WA, USA), α -SMA (1:100, NB300-678, Novus), ARG-1 (1:200, LS-C447907, LS Bio), and/or iNOS (1:200, GTX17504, Genetex), MYH-11 (1:200, NBP2-44532, Novus) overnight at 4 °C. After thrice PBS washing, samples were incubated with secondary antibodies including anti-rabbit Alexa Fluor 488 and 594 (1:1000, 111-545-003 and 11A1-585-003, Jackson ImmunoResearch Laboratories), anti-

goat Alexa Fluor 488 (1:1000, A11055, Invitrogen), and/or anti-mouse Alexa Fluor 594 (1:1000, A11005, Invitrogen) for 2 h in the dark. After 3 times PBS washing for 10 minutes each, confocal imaging (LSM 780, Zeiss) was conducted after nucleus staining.

2.20. Data analysis

All experimental data are presented as mean \pm standard deviation (SD), with 'n' denoting the number of samples. These samples were obtained from more than three independent experiments, or with dots and whisker plots, in which dots and whiskers are shown as average and minimum/maximum, respectively. For pairwise comparisons, the unpaired Student's t-test was used, while multiple-group comparisons were assessed using a one-way analysis of variance (ANOVA). Post-hoc analyses, including Bonferroni's and Tukey's methods, were employed to explore group-wise differences. Significance levels were denoted by p-values (*p < 0.05, **p < 0.01, and ***p < 0.001). All statistical analyses were performed with the following software programs: Excel, SigmaPlot (V12.0, Systat Software Inc., San Jose, CA, USA), MATLAB (Mathworks, USA), and GraphPad Prism 5 (San Diego, CA, USA). Quantitative image analyses including color image processing, were conducted using ImageJ software (Fiji, National Institute of Health, MD, USA).

3. RESULTS

3.1. Development of Artificial vasa-vasorum (AVV)

The vascular grafting system with AVV in this study consists of two components: (i) a decellularized artery vascular graft with heparin immobilization surface coating, and (ii) an artificial vasa-vasorum enveloping the tunica adventitia of the blood vessel with a 3D Microchannel network hydrogel (**Figure 1a**). The microchannel network, which plays a key role in mimicking the function of the vasa vasorum, is fabricated using a technique that involves (i) uniformly extracting microfibers with a size of 20-40 μm and (ii) utilizing phase change at below the lower critical solution temperature (LCST = 32 $^{\circ}\text{C}$) of poly (N-isopropylacrylamide) (PNIPAM). PNIPAM solution is utilized to form microfibers through a spinning machine, resulting in an average diameter of the microchannels measured at $14.94 \pm 5.81 \mu\text{m}$ as confirmed by SEM image analysis (**Figure 2**).

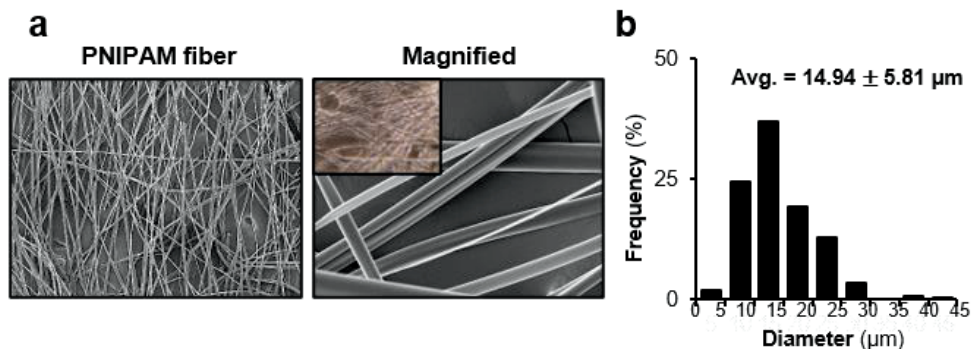


Figure 2. PNIPAM fiber mimicking structural function of capillary vessel.

Artificial vasa-vasorum-incorporated vascular grafting system follows the fabrication steps outlined below: (i) Preparation of decellularized artery scaffold with surface coating technique (**Figure 3a**). (ii) Sterilization and preparation of 5.5 w/v% gelatin hydrogel along with m-transglutaminase (mTG) for crosslinking (**Figure 3b**). (iii) Placement of the blood vessel at the center of Polydimethylsiloxane (PDMS) mold, followed by embedding the gelatin hydrogel with PNIPAM fiber into a cylindrical space around vascular scaffold, maintaining a temperature above the lower critical solution temperature (LCST = 32 $^{\circ}\text{C}$) (**Figure 3c**). (iv) After gelatin-mTG

crosslinking at 37 °C for 30 minutes, lowering the temperature to below the LCST and immersing the hydrogel with PBS, causing PNIPAM fiber to dissolve, leading to the formation of a microchannel network (**Figure 3c**). The microchannel network structure in hydrogel was confirmed through channel staining by 0.1 μm bead perfusion. The artificial vasa-vasorum, wraps around the outer layer of the decellularized scaffold, providing a structural and functional emulation of vasa-vasorum responsible for blood flow, oxygen, and nutrient supply.

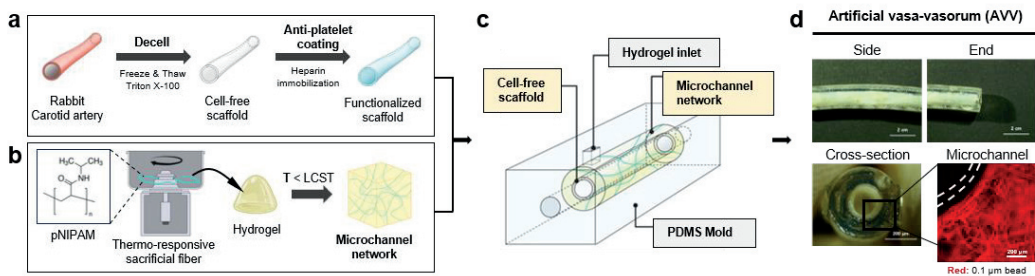


Figure 3. Fabrication step and gross appearance of artificial vasa-vasorum with cell-free scaffold.

3.2. Decellularized vascular scaffold protocol and surface modification.

Decellularized vascular scaffolds have shown promising outcomes in several pre-clinical studies²⁸. Comparative investigation to explore optimal methods aimed at minimizing the loss of ECM structural integration and mechanical strength during the decellularization process. The first method involved a chemical-chemical approach, where we applied a short exposure to a non-ionic detergent after treating the extracellular matrix with the ionic detergent SDS. The second method utilized a mechanical-chemical approach, where non-ionic detergent was treated following freeze-thaw cycles (Figure 4a). In the chemical-chemical approach group, SDS was applied for 48 hours, followed by a 12-hour treatment with Triton X-100, with continuous perfusion of vascular inner detergent within a bioreactor. On the other hand, the mechanical-chemical method involved subjecting the graft to five cycles of temperature variation, alternating between liquid nitrogen and 37°C PBS, followed by a 12-hour Triton X-100 perfusion. All samples were lyophilized for long-term storage. Nucleus staining using 4',6-diamidino-2-phenylindole (DAPI) demonstrated successful removal of cellular components in

both protocols (**Figure 4b**). Additionally, quantification of double-stranded DNA and western blot analysis provided further evidence for the results (**Figure 4c**). The western blot results revealed that endothelial cells (CD31) and vascular smooth muscle (VSMC) components were successfully removed during the decellularization process, while the type 1 collagen which is major component of tunica adventitia, was similarly preserved in both protocol (**Figure 4d**). However, the SDS-based decellularization process resulted in the loss of glycosaminoglycan (GAG) components, which play an important role in the structural integration of the extracellular matrix and promote cellular growth and differentiation. This loss is attributed to the negative charge of sulfate and carboxylate present in GAG, which is compromised by ionic detergent SDS. Quantification of sulfated GAG revealed that the mechanical-chemical method better preserved sGAG content than chemical-chemical method (**Figure 4e**).

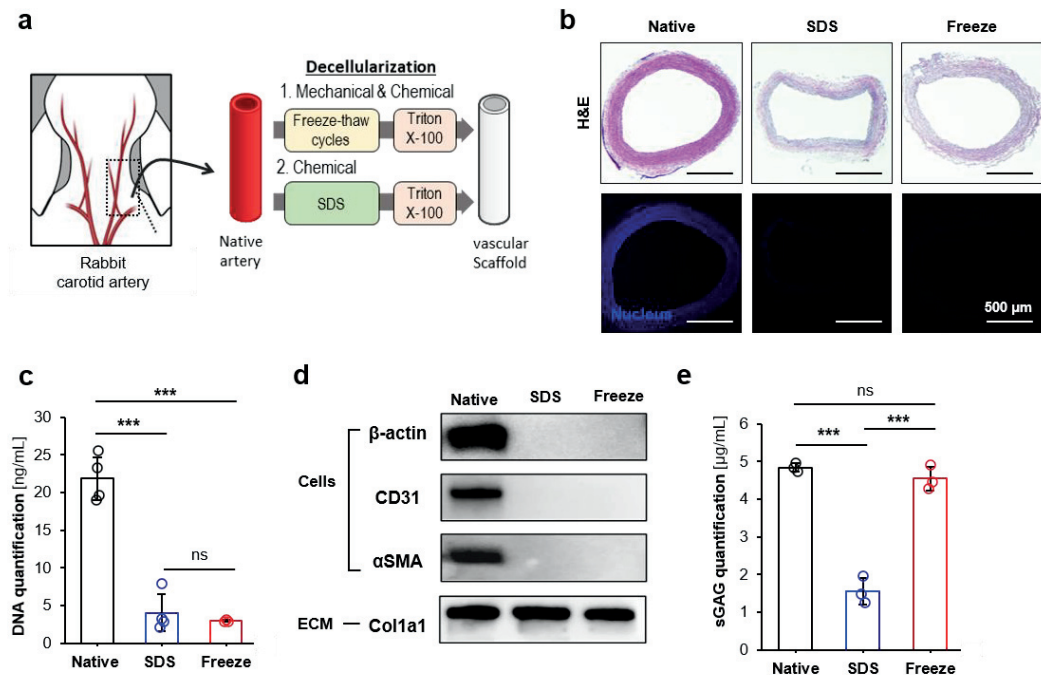


Figure 4. Investigation of Decellularization Methods for Vascular Scaffolds and characterization.

We investigated how the mechanical properties are affected by different decellularization

methods through tensile test. The histological structure of blood vessels is composed of three layers: (i) the tunica intima, which contains endothelial cells, (ii) the tunica media, consisting of smooth muscle and elastic fibers, (iii) and the tunica adventitia, which surrounds the blood vessels with collagen fibers and glycosaminoglycans. The mechanical properties of blood vessels in the radial direction respond differently to pressure changes. At low strains, the tunica media exhibits elastic behavior dominantly, contributing to the vessel's ability to stretch and recoil. At under high strains, the tunica adventitia plays a main role by providing robust support. These two properties collaborate to give the blood vessel a hyperelastic characteristic, similar to that of a rubber band (**Figure 5a**). The maximal strain value obtained from the strain-stress curve reflects the characteristics of vascular smooth muscle cells (VSMCs) and elastin, while the tangent modulus and ultimate tensile strength shows the properties of the collagen structure. Both the SDS and Freeze-thaw cycle method effectively removed cellular components from the native artery, resulting in a similar reduction in maximal strain due to the loss of smooth muscle cells. However, the Freeze-thaw cycle group demonstrated significantly higher tangent modulus and ultimate tensile strength compared to the SDS-based chemical decellularization protocol, providing evidence of collagen structure preservation (**Figure 5b, c**).

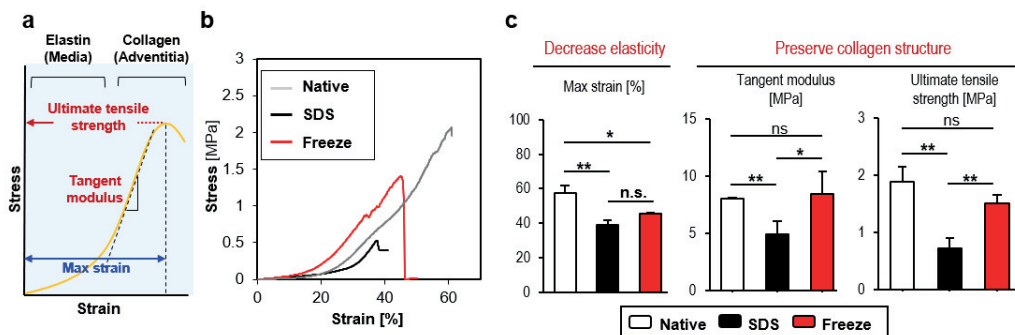


Figure 5. Effect on radial tensile strength of vascular scaffold by decellularization protocols.

3.3. Heparin immobilization for anti-thrombotic coating

To prevent early thrombosis due to platelet activation caused by direct exposure of the basement membrane in the vascular lumen after implantation, heparin immobilizing process was employed. The EDC and NHS reaction facilitated the crosslinking of heparin with the decellularized artery scaffold, promoting amide bond formation to immobilize heparin within

the luminal side of vessel. Quantitative results from toluidine blue staining demonstrated successful heparin immobilization through the EDC and NHS crosslinking process (**Figure 6a**). Mouse plasma-rich platelets were treated to the vascular scaffold and subjected to SEM imaging to quantify the number of adhered platelets and assess their activation level. The group with heparin immobilization showed a reduced number of platelets and decreased activity compared to the non-heparin-coated group (**Figure 6b**).

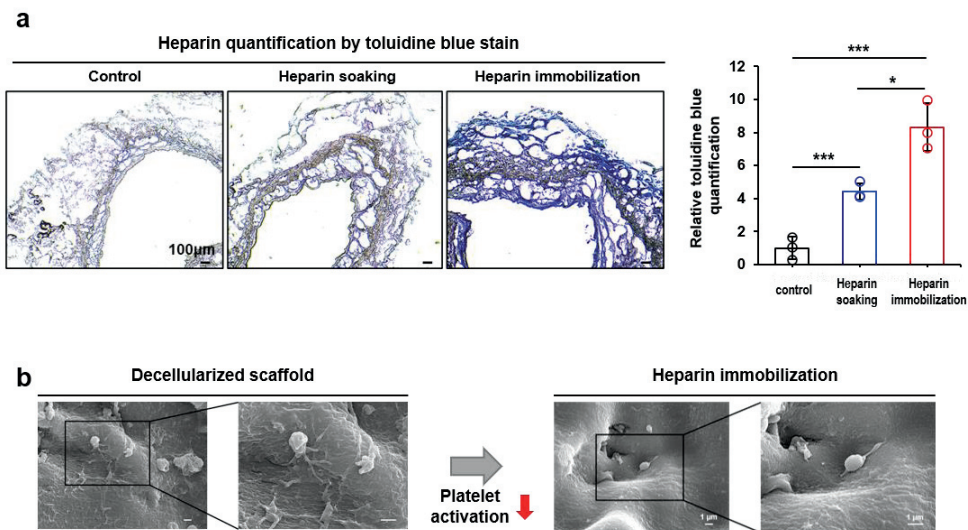


Figure 6. Anti-thrombosis effect of heparin immobilization

3.4. Artificial vasa-vasorum as a structural and functional vasculature.

Artificial vasa-vasorum not only serves a functional role in promoting the supply of oxygen and nutrients to the scaffold through its capillary network in an in-vivo environment but also induces actual endothelial cell tube formation. For investigating beneficial effects, AVV was implanted in the rabbit carotid artery for 14 days, and perfusion and diffusion-based confocal image analysis were performed. The results clearly demonstrated increased Fluorosphere (red) perfusion-bead signal and FITC-dextran (40kDa) diffusion capacity within the microchannel network group of the hydrogel (**Figure 7a**). To explore the capability of AVV in supporting endothelial cell recruitment and vascular tube formation, we conducted a 7-day perfusion-based

culture of human induced pluripotent stem cell-derived endothelial cells (hiPSC-EC)²⁶ within cylinder-shaped AVV. The experimental group was divided into channel (+) and (-). Imaging analysis using confocal microscope imaging successfully describe endothelial cell tube formation within the microchannel network (**Figure 7b**).

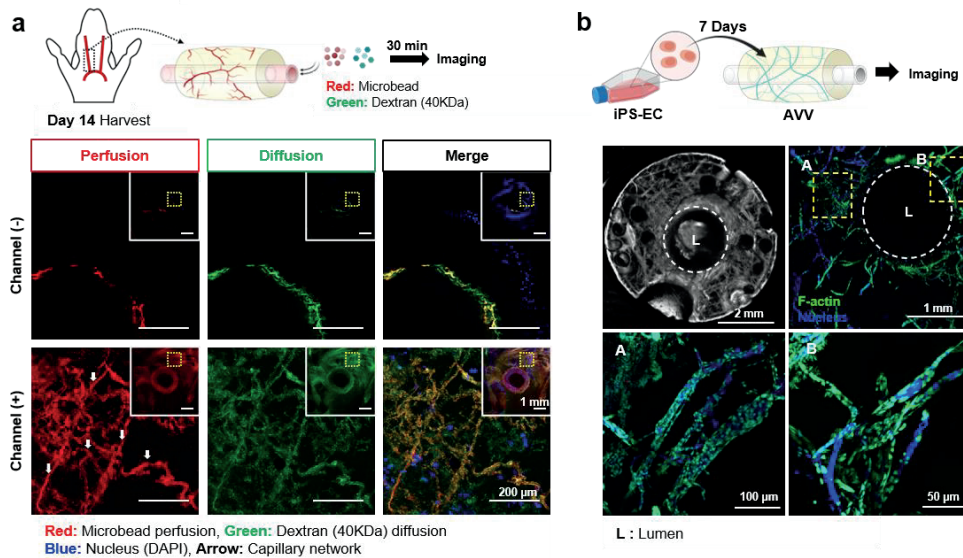


Figure 7. AVV Promote perfusion and diffusion capacity and EC tube formation

3.5. *In-vivo* performance of AVV

To demonstrate the increased patency and regenerative effects of AVV in implantation of small-diameter artificial blood vessels (< 6mm), we developed a Rabbit carotid interposition model. The animal experiment involved performing end-to-end anastomosis by connecting the allograft cell-free scaffold with artificial vasa-vasorum (AVV) to the right carotid artery of rabbits (**Figure 8a**). To evaluate the effect of the microchannel network, the experimental groups were divided into those with channels within the hydrogel and those without channels (n=15 each group). The groups were further divided based on the time of evaluation at 7 days, 14 days, and 30 days (n=5 each group) to assess inflammation and scaffold regeneration effects over time. Doppler sonography was conducted for blood flow measurements, and angiography and histological analysis were performed at each time point (**Figure 8b**).

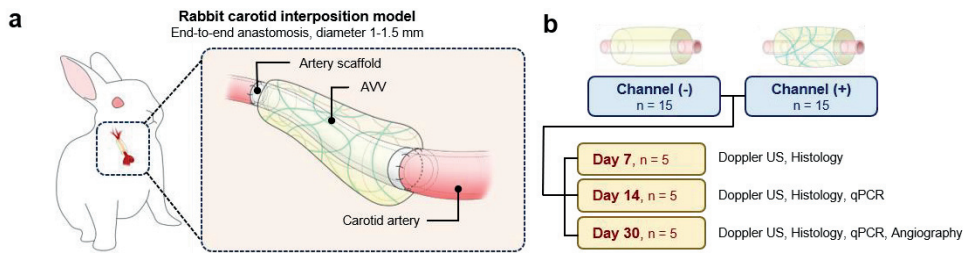


Figure 8. Schematic illustration of animal study

All cases that underwent surgery showed patent blood flow in doppler sonography. On the 14th day after surgery, gross appearance of AVV and graft revealed that the channel-positive hydrogel showed filling of blood vessels and tissues within the hydrogel. In contrast, the group without channels showed no vascularization within the hydrogel (**Figure 9a**). In addition the results of the 30-day angiography demonstrated that AVV can enhance the long-term patency of the small-diameter cell-free scaffold (**Figure 9b**).

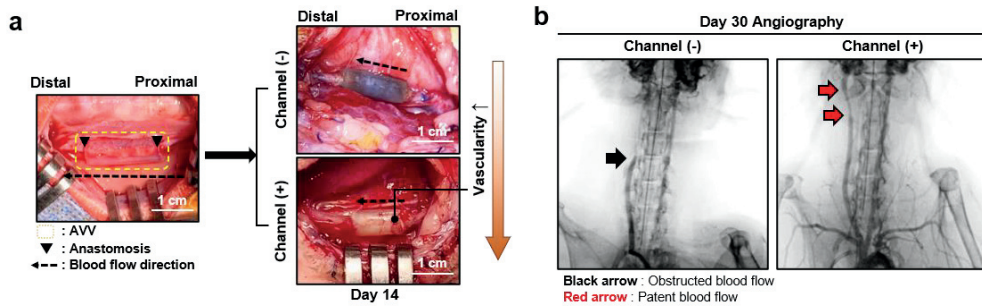


Figure 9. Gross appearance of day 14 post operation and angiography images of rabbit carotid interposition model.

Histological analysis validates the performance of the cell-free vascular graft based on the presence or absence of microchannels. Hematoxylin-eosin staining results showed that at day 7, the hydrogel surrounding the blood vessels remained intact, but by approximately day 14, degradation and inflammatory reactions occurred. By day 30, the hydrogel disappeared, and vascular remodeling was observed. The Channel (-) group exhibited intraluminal thrombosis

at day 7, and neointima formation at day 14, and total obstruction due to neointima at day 30 (Figure 10a). Luminal area measurements based on histology demonstrated AVV's stenosis prevention effect in the channel (+) group (Figure 10b). Analysis of the histological findings showed a higher incidence of early thrombosis (Day 7) in the channel (-) group compared to the channel (+) group, and at days 14 and 28, neointima formation was more pronounced in the channel (-) group (Figure 10c).

Doppler sonography results exhibited higher peak velocity and lower back flow formation in the channel-positive group (Figure 10d). Quantitative data confirmed the advantageous effect of AVV on graft patency, with no cases of complete obstruction observed in the channel (+) group (Figure 10e), providing strong evidence for the efficacy of AVV in maintaining long-term patency of the small-diameter cell-free scaffold.

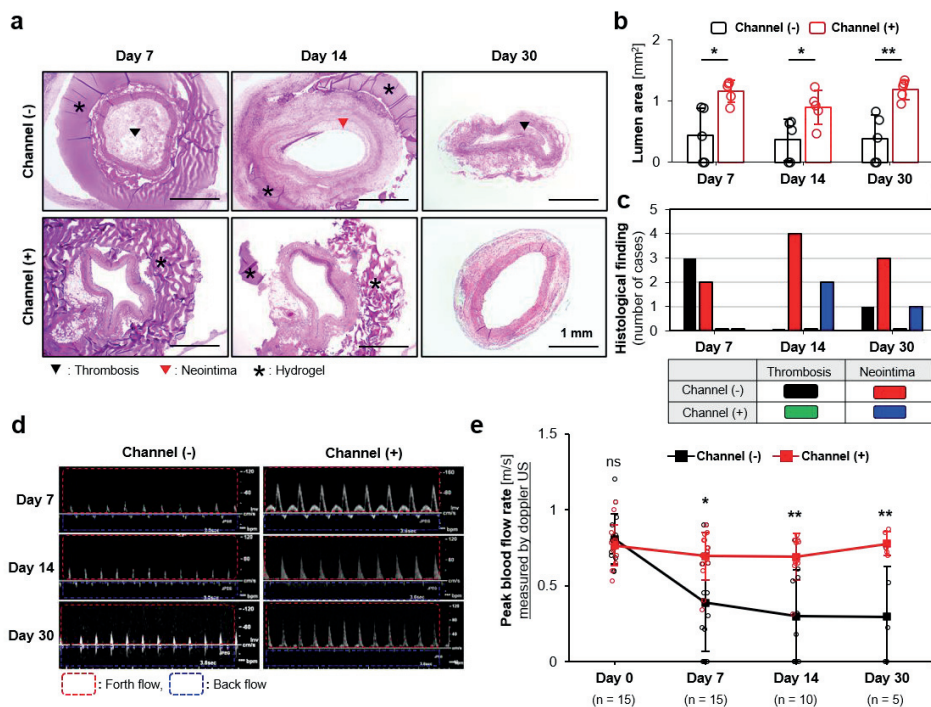


Figure 10. Histological analysis and blood flow data for AVV in rabbit carotid artery interposition model.

3.6. “Inside-out” and “Outside-in” re-endothelialization of cell-free scaffold

To evaluate the cellular recruitment ability and re-endothelialization capability of AVV to cell-free scaffold, we performed immunostaining for endothelial cells (CD31) and monocytes (CD11b) on artery tissues at 7 and 14 days after carotid artery interposition procedure. The process of EC restoration by AVV vascular scaffold occurs in a two-step process: i) early luminal reendothelialization (inside-out), which is promoted by the recruitment of endothelial progenitor cells (EPCs) and monocytes, and ii) late vascularization of the scaffold (outside-in), achieved by the vascular formation ability of M2 macrophages (**Figure 11**). These two effects are orchestrated to ultimately inhibit early thrombosis and late neointima formation.

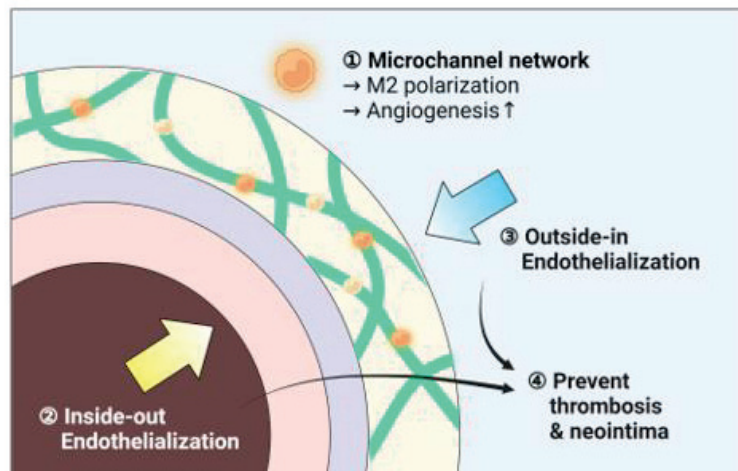


Figure 11. Schematic illustration of inside-out and outside-in re-endothelialization

The histopathological and immunostaining results in 7-day group demonstrate that the channel (+) group promotes re-endothelialization within the lumen of the cell-free scaffold. In contrast, the channel (-) group fails to re-endothelializing luminal space, leading to a higher incidence of thrombosis and obstruction. Additionally, recruitment of CD11b positive cells was observed in lumen. At day 14, the immunostaining results show that the channel (-) group exhibits stenosis due to neointima formation, with minimal recruitment of CD31 and CD11b positive cells. On the other hand, the channel (+) group displays active cellular recruitment from the

outer region of the scaffold, with the majority of these cells being endothelial and mononuclear cells (**Figure 12a**). Quantitative analysis of fluorescent intensity provides evidence for two main functions of AVV: (i) enhancing early reendothelialization (inside-out) and late vascularization around scaffold (outside-in), and (ii) promoting recruitment of monocyte cells, which play a key role in mediating these regenerative processes (**Figure 12b**).

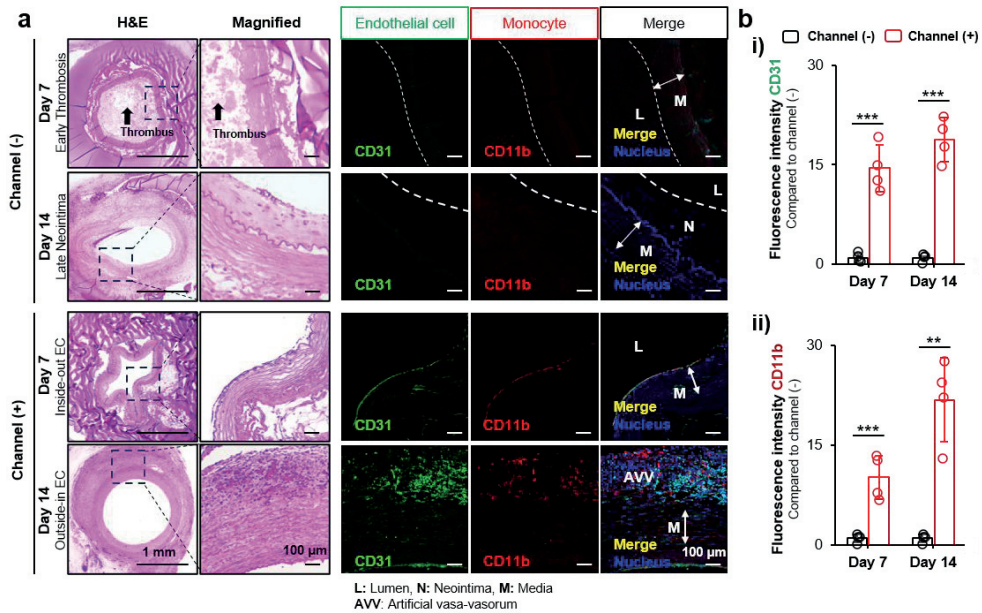


Figure 12. Histology and immunostaining result validate re-endothelialization capability of AVV

The gene expression analysis conducted through QPCR on harvested vascular grafts further verified the angiogenic potential of AVV. At both the 7-day and 14-day time points, an increase in the expression of endothelial cell markers (CD31) and endothelial progenitor cell markers (CD34, CD133) was demonstrated. This provides additional evidence of AVV's ability to promote angiogenesis(**Figure 13**).

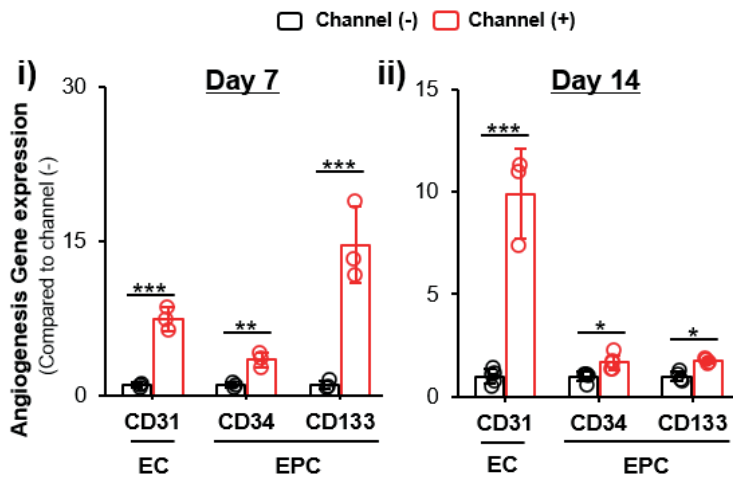


Figure 13. Angiogenic potential of AVV recruit EC and EPC to cell-free scaffold.

3.7. *In vivo* Macrophage M2 polarization by AVV

To investigate the function of recruited inflammatory cells in the vascular scaffold's vascularization, immunostaining and gene expression analysis were performed for macrophage polarization-related markers. The fluorescence quantification analysis showed that on Day 14, the Channel (+) group exhibited enhanced recruitment of monocytes and an increased expression of M2 phenotype markers compared to M1 phenotype markers (**Figure 14a, b**). Additionally, these results were supported by the higher expression of M2 markers (IL-10, ARG-1) and lower expression of M1 markers (IL-1 β , TNF- α) in the channel (+) group (**Figure 14c**).

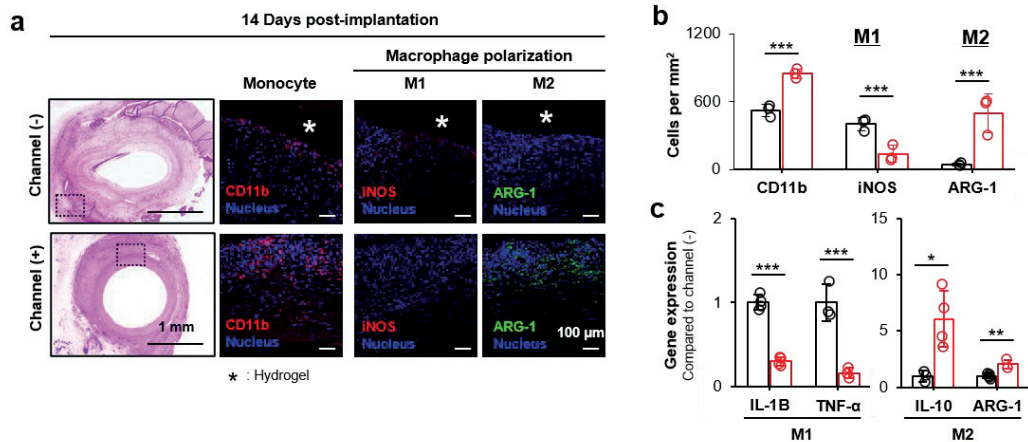


Figure 14. *In vivo* macrophage phenotype modulation effect of AVV.

3.8. *In vitro* macrophage phenotypic modulation by microchannel network

To investigate the macrophage phenotypic modulation by microchannel network, macrophage cells (RAW 264.7 cell) were 3D-cultured on gelatin-based hydrogel, and protein and gene expression were investigated using immunostaining and QPCR. Disc-shaped gelatin-mTG crosslinked hydrogels were prepared, and the groups were divided based on the presence or absence of microchannels. Raw 264.7 cells were seeded on the discs, and after 7 days of culture, the results of F-actin staining showed that mononuclear cells infiltrated into the microchannel and formed an aligned and packed cellular structure, while in the group without microchannels, cells attached onto top surface of the hydrogel (**Figure 15a**). The experimental process involved seeding cells onto the hydrogel on Day 0, following LPS treatment for macrophage activation on Day 2, and conducting imaging studies on Day 7 (**Figure 15b**). Immunostaining images and fluorescence quantification results for M1 (iNOS) and M2 (ARG-1) macrophage markers demonstrated that macrophages infiltrated into the microchannel network were polarized towards the M2 phenotype (**Figure 15c, d, e**). Gene expression analysis representing macrophage polarization showed that the microchannel-positive group exhibited decreased expression of M1 markers (IL-1B, iNOS, TNF α , IL-6) and increased expression of M2 markers (CD 206, CD163, IL-10, ARG-1, TGF-IL-10, ARG-1, TGF- β) (**Figure 15f**). These results

validate that the microchannel network not only promotes cellular inflammatory recruitment but also induces macrophage M2 polarization through mechanotransduction.

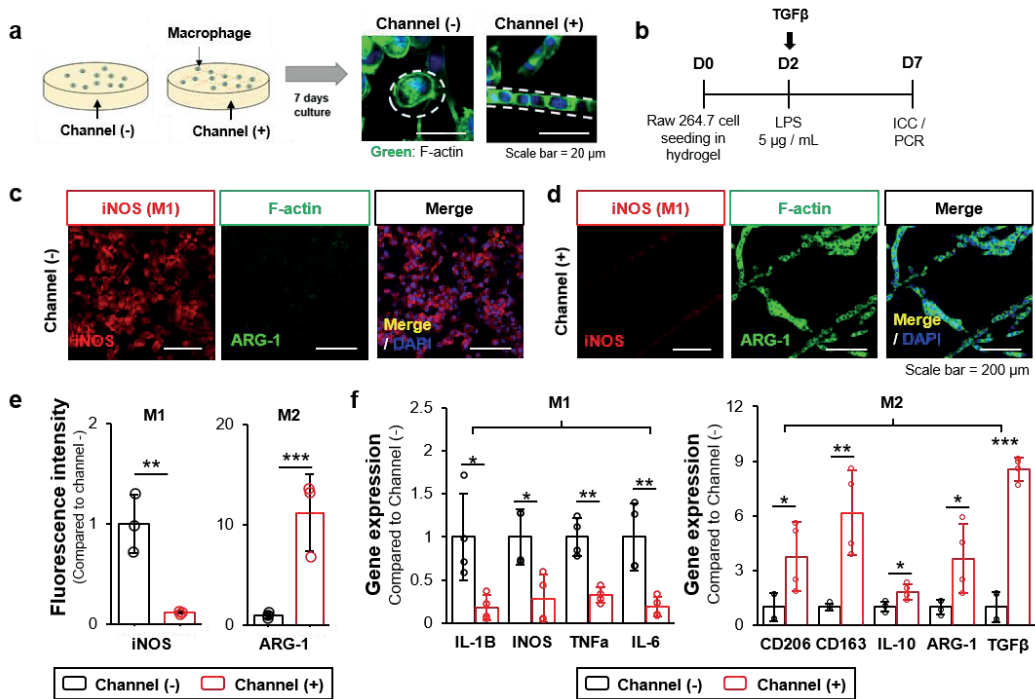


Figure 15. Microchannel network promote M2 macrophage polarization.

3.9. *In-vitro* EPC migration assay

In vivo experimental results demonstrated the important role of endothelial progenitor cells (EPCs; CD34, CD133 positive cells) and monocytes (CD11 positive cells) during the early luminal re-endothelialization process. Based on these findings, we hypothesized that the microchannel network's inflammation modulating capability could enhance the luminal recruitment of circulating EPCs via angiogenesis related chemoattractant (**Figure 16a**). To validate this early endothelialization effect, we conducted a migration assay of EPCs with mouse macrophages (Raw 264.7 cells) embedded into the hydrogel. (**Figure 16b**). The results confirmed that AVV with microchannels effectively promoted EPC migration, as demonstrated by tracking the migration area after 14 days of culture (**Figure 16c, d**).

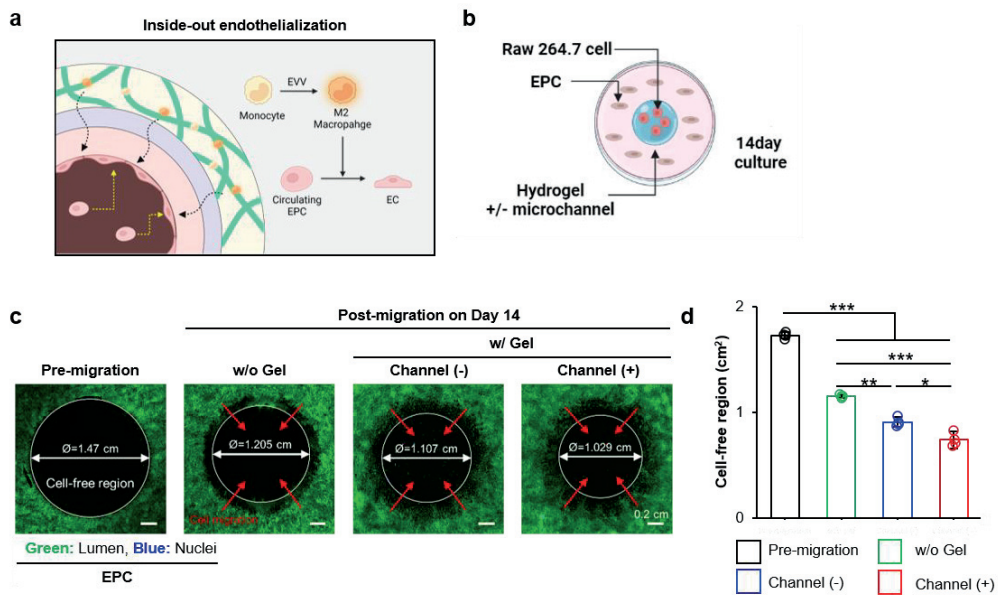


Figure 16. Radius EPC migration assay demonstrate the mechanism of early re-endothelialization

3.10. VSMC restoration and vascular remodeling after day 30 post-implantation

In order to enhance the long-term patency of the tissue-engineered vascular graft (TEVG), the restoration and remodeling of vascular smooth muscle cells (VSMCs) within the vascular scaffold, as well as the recovery of elasticity are essential. H&E staining results at Day 30 and immunostaining for contractile VSMC-specific markers (α SMA, MYH-11) confirmed that smooth muscle restoration into the tunica media was promoted by the AVV (**Figure 17**).

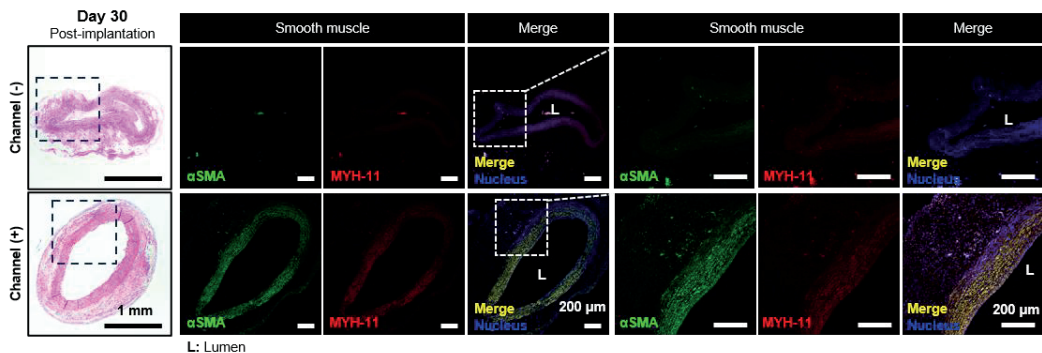


Figure 17. VSMC restoration and vascular remodeling at day 30 post-implantation.

The quantification of fluorescent intensity demonstrated an increased expression of contractile vascular smooth muscle cells (VSMCs) in the microchannel network group (Figure 18a). The result was supported by the higher gene expression levels of VSMC markers (α SMA, SM22 α) in the channel (+) group. Additionally, we focused on TGF- β as a pivotal player in these VSMC regeneration processes and QPCR result demonstrated increased gene expression in the channel (+) group (**Figure 18b**).

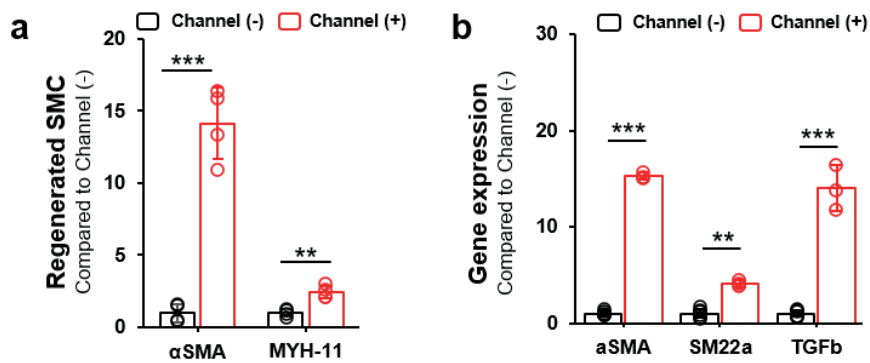


Figure 18. Comparing protein and gene expression level of VSMC restoration.

In the process of vascular remodeling, perivascular mesenchymal stem cells (MSCs) and macrophage are considered an important player in restoration of vascular smooth muscle cells (VSMCs). M2 polarized macrophages promoting this differentiation through activated TGF- β

signaling. We conducted in vitro trans-well study for elucidating the differentiation and regeneration process (**Figure 19**).

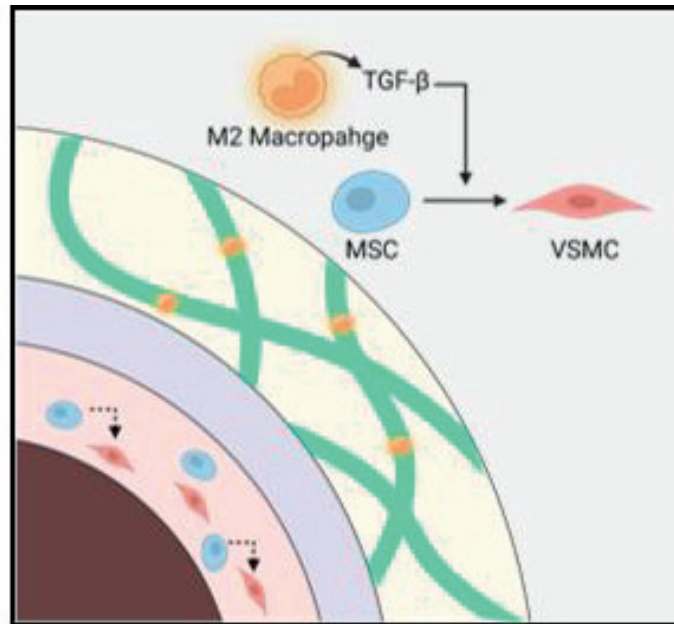


Figure 19. VSMC differentiation from MSC was promoted by TGF- β signaling of M2 macrophage

3.11. *In vitro* VSMC differentiation from hMSC promoted by microchannel network.

To investigate the potential of MSCs in inducing VSMC differentiation within the AVV, a trans-well study was conducted. In this experiment, hydrogels with or without channels were cultured with Raw 264.7 cells in the top chamber for 2 days, followed by LPS treatment for activation. After 2 days, hMSCs were seeded in the bottom chamber, and trans-well co-culture was performed. Immunostaining, QPCR, and supernatant ELISA for TGF- β were then carried out (**Figure 20a, b**). Immunofluorescence staining images for the vascular smooth muscle marker (α SMA) provided evidence of MSCs' VSMC differentiation induced by M2 macrophages (**Figure 20c**). The gene expression analysis for contractile phenotype SMC

(α SMA, SM22 α) further supported the results (**Figure 20d**). Moreover, the analysis of TGF- β levels, a key player in this differentiation process, was measured by ELISA using media supernatants at day 7. The results showed that the microchannel network hydrogel group had higher concentration level of TGF- β (**Figure 20e**).

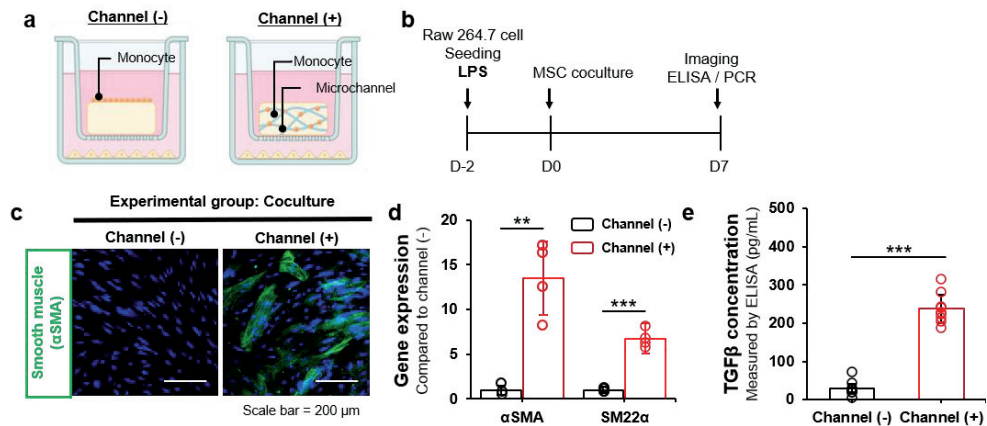


Figure 20. In vitro trans-well study for elucidating the mechanism of VSMC restoration.

3.12. Regenerated elasticity of cell-free scaffold by VSMC restoration.

To evaluate the mechanical function of the vascular smooth muscle, a radial tensile test was performed at day 30 post-implantation (**Figure 21a**). The clear increase in tensile strain at break in channel (+) group from day 0 (green) to day 30 (red) observed in the stress-strain curve demonstrates an enhancement in elasticity attributed to the recovery of cellular components in the tunica media (**Figure 21b**). Although there was no significant difference in Young's modulus of the tunica adventitia during the remodeling process, there were statistically significant increase in tensile strain and stress at break between the two groups (**Figure 21c**). The results evidenced that AVV promoted successful VSMC restoration during vascular remodeling process.

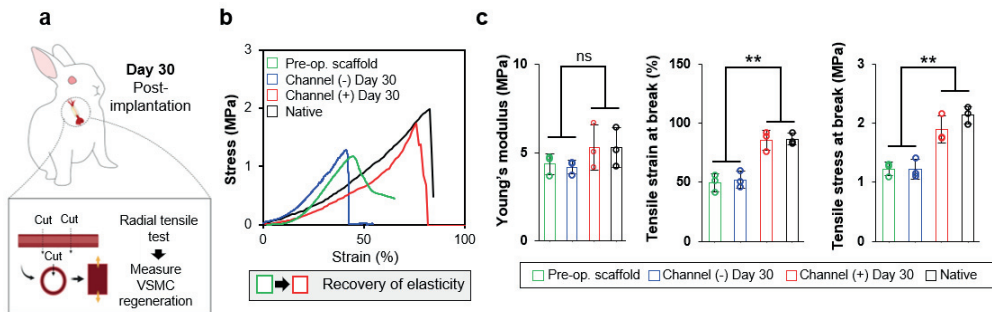


Figure 21. Ex-vivo tensile test to investigate VSMC restoration.

3.13. Versatile utility of AVV

AVV facilitates early re-endothelialization and tissue regeneration by regulating inflammation and promoting scaffold vascularization, thereby enhancing VSMC restoration and inducing successful remodeling. To evaluate the versatility and diverse utility of AVV, additional surgical models were established. In the case of rabbit carotid arteries, with a size of 1.5-2.5 mm, it serves as a model consistent with human coronary arteries or below-knee arteries in peripheral artery disease. However, in case of microsurgery procedures, such as reconstruction surgery or flap surgery, may involve anastomosis of vessels smaller than 1 mm. To address this, we developed a rabbit femoral artery end-to-end anastomosis model for vessels smaller than 1 mm (**Figure 22a**). The gross appearance at day 14 post-operation demonstrated that the microchannel network group exhibited enhanced hydrogel vascularization (**Figure 22b**).

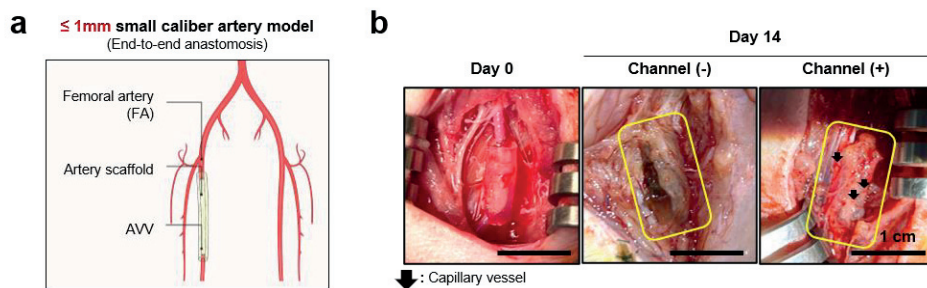


Figure 22. Rabbit femoral artery model for end-to-end anastomosis of very small artery ($\leq 1\text{mm}$).

The H&E staining results demonstrated that the channel (-) group had a diameter of 670 μm , while the channel (+) group had a diameter of 810 μm , confirming the presence of very small-sized vessels in the model. In the channel (+) group, we observed the presence of restored cells inside the scaffold, while in the channel (-) group, neointima formation occurred, but no cell infiltration was observed within the vascular scaffold (**Figure 23a**). Quantitative analysis of the luminal area demonstrated that AVV could increase patency even in vascular models with a diameter of less than 1 mm (**Figure 23b**). This finding was further supported by measurements of vascular diameter from angiography (**Figure 23c**) and peak velocity from Doppler sonography (**Figure 23d**).

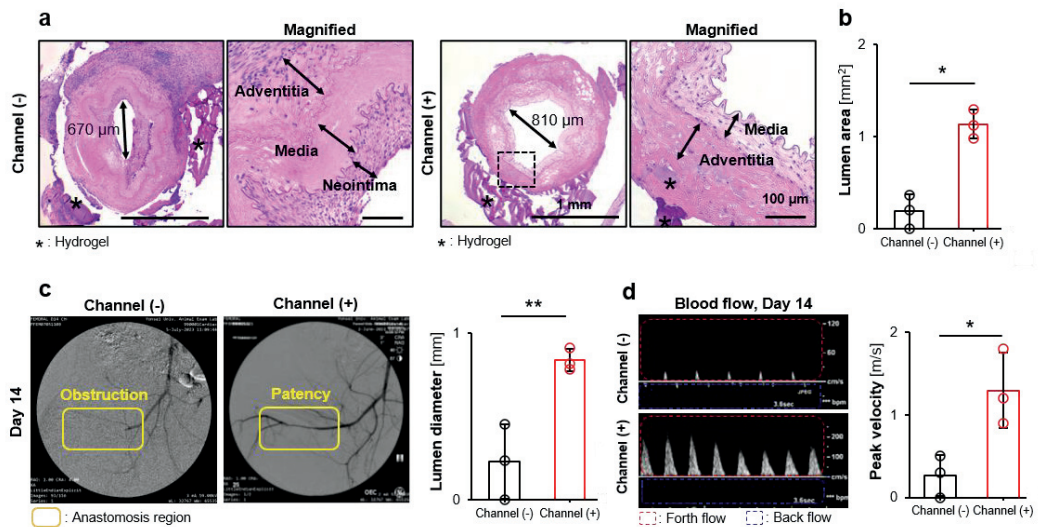


Figure 23. Effects of AVV on $\leq 1\text{mm}$ sized vascular grafting models: Histological and Functional Analysis

Additionally, to assess the utility in models with end-to-side anastomosis, we established a bypass surgery model in rabbits, connecting the descending aorta to the common iliac artery (**Figure 24a**). AVV successfully functioned in the end-to-side model without disrupting blood flow, and the angiography and sonography results at day 14 showed maintained patency even two weeks after the procedure (**Figure 24b, c**).

4. DISCUSSION

Biological actions at all levels including organ, tissue, cell, and molecule occurs in a cascade fashion, which can be applied to interpret not only pathogenesis but also regeneration. Organ functions are operated by decision-maker cells in collaboration with hardware cells. In these aspects, most therapeutic and regenerative strategies to handle the vascular pathophysiology have been targeted to the lumen-intima side with expectation to exert the cascade effects on the vessel wall based on the concept of inside-out control. For the past decades, much less attention has been paid to the opposite direction of strategies (outside-in control). This study is aligned with this paradigm-shift to focus on the vasa-vasorum of vascular out wall as an onsite recruiter of vascular cells for the inside regeneration of the decellularized scaffold. The regenerative actions propagate from AVV to the smooth muscle layer with the pro-endothelialization effect. The catalyst action to initiate this cascade effect is the microchannel-mediated M2 polarization of macrophages, which is effective enough to maintain the patency in the three models of small vessel grafting (< 6 mm in diameter).

When macrophages invade into the microchannel network whose diameter is a cell-size, the slowed cell migration results in packing with alignment like a motorcade in a small tunnel. This physical setting forces M2 polarization of macrophages by mimicking EC lining in a blood vessel. In this way, regenerative paracrine signals are produced to recruit E(P)Cs from both luminal and adventitial sides for endothelialization of intimal and AVV. Also, the production of TGF- β through the M2 polarization appears to cause the differentiation of precursor cell such as pericyte and MSCs to SMCs, which is synergized in collaboration of the endothelialization. This study presents a considerable value because the easily accessible design of AVV graft is used to validate the complex mechanism of cascade regeneration. As the mechanism affects cellular restoration and repair in a layer-by-layer fashion throughout the vessel wall, a meaningful solution is suggested in agreement to the outside-in control paradigm as seen in current research on vascular pathophysiology. Moreover, the channel network physically drives the morphological change of macrophages as a decision-maker, indicating that the 3D pattern can guide a series of cellular responses in a cause-and-effect manner. Hence, this study serves as a real model of biomedical engineering to translate the engineering technology to the clinical side by controlling the

biological mechanisms following the theme of structure-function relationship.

The development of small vascular graft (< 6mm diameter) has been an unmet subject of extensive research for the decades. Continuous progress has been made in using biocompatible materials, manufacturing techniques, and re-cellularization methodology². The key point of successful regeneration is to restore the intact tissue structure and cellular composition like the native vessels. Hence, the decellularized vessels have been a promising subject following the concept of allograft as the ECM composition is at least preserved. A variety of decellularized xenografts have been tested for clinical applications of arteriovenous access (e.g., Artegraft®; bovine carotid artery, SynerGraft®; bovine ureter, etc.). However, unsatisfactory outcomes are reported in relation to side effects such as thrombosis and aneurysm³. Similar vascular grafts are made using porcine small intestinal submucosa (SIS), such as CormMatrix®, resulting in stenosis of small-diameter vessels⁴. When the lessons of trials are considered, the present study approaches a simple but impactable strategy as the decellularization method is tuned to preserve the ECM composition including collagen and GAG. AVV induces restoration of cellular composition by preventing thrombosis through heparin immobilization like setting up the software to the well-structured hardware.

Although the successful maintenance of patency is reported in the three models of small vessel grafting, further studies are needed in examining the long-term patency for more than years. Since the current study focuses on the AVV effect on cellular restoration and the application utility for different sizes (<1, ~3, and >3 mm) of vessel grafting, the endpoint analyses end up before the gel degradation is completed within a month. In addition to the known report-based examination of TGF- β effect on SMC restoration, the key paracrine signals from the M2 polarization need to be determined through the omics or systemic analyses in the next study because multi-way synergistic actions among the regenerative cytokine and growth factors are expected to involve the pro-endothelization. Nonetheless, this study approaches a variety of new experiment models to validate the AVV function as most challenging point so that more insight generation can be facilitated in the series of future studies.

5. CONCLUSION

The study highlights a paradigm shift that emphasizes the vascular out-wall over the lumen intimal factors, revealing the significant role of “vasa vasorum” in mediating interactions within the vascular wall. In an adventitial (outside-in) side concept, AVV is engineered within an implantable hydrogel, forming microchannel networks. This unpredictable approach comes after extensive validation studies on implantation functions. When AVV is employed to encase the external wall of a cell-free scaffold, which is prepared through post-decellularization, it ensures retention of vital mechanical properties. In rabbit artery implantations, both inter-positional and bypassing, the AVV graft proves pivotal in recruiting vascular cells to the cell-free wall. It achieves this by stimulating the invasion of angiogenic and vasculogenic cells, facilitated by the M2 polarization of macrophages. This dynamic process leads to the effective restoration of smooth muscle cells, revitalizing vascular elasticity and ensuring prolonged graft patency. In essence, the AVV emerges as a groundbreaking catalyst for vascular wall regeneration, setting the stage for potential clinical successes in small-diameter vascular grafting.

References

1. Tsao CW, Aday AW, Almarzooq ZI, Alonso A, Beaton AZ, Bittencourt MS, et al. Heart disease and stroke statistics—2022 update: a report from the American Heart Association. *Circulation* 2022;145:e153-e639.
2. Go AS, Mozaffarian D, Roger VL, Benjamin EJ, Berry JD, Borden WB, et al. Heart disease and stroke statistics—2013 update: a report from the American Heart Association. *Circulation* 2013;127:e6-e245.
3. Popov G, Vavilov V, Popryaduhin P. Is it Possible to Create Readily Available Tissue-Engineered Vascular Grafts Without Using Cells? *European Journal of Vascular and Endovascular Surgery* 2019;58:e190-e1.
4. Raza S, Chang C, Deo SV, Sabik JF. Current role of saphenous vein graft in coronary artery bypass grafting. *Indian Journal of Thoracic and Cardiovascular Surgery* 2018;34:245-50.
5. Niklason L, Gao J, Abbott W, Hirschi K, Houser S, Marini R, et al. Functional arteries grown in vitro. *Science* 1999;284:489-93.
6. Weinberg CB, Bell E. A blood vessel model constructed from collagen and cultured vascular cells. *Science* 1986;231:397-400.
7. Peck M, Gebhart D, Dusserre N, McAllister TN, L'Heureux N. The evolution of vascular tissue engineering and current state of the art. *Cells Tissues Organs* 2011;195:144-58.
8. Yuan H, Chen C, Liu Y, Lu T, Wu Z. Strategies in cell-free tissue-engineered vascular grafts. *Journal of Biomedical Materials Research Part A* 2020;108:426-45.
9. Isenberg BC, Williams C, Tranquillo RT. Small-diameter artificial arteries engineered in vitro. *Circulation research* 2006;98:25-35.
10. Badylak SF, Freytes DO, Gilbert TW. Extracellular matrix as a biological scaffold material: Structure and function. *Acta biomaterialia* 2009;5:1-13.
11. Gui L, Muto A, Chan SA, Breuer CK, Niklason LE. Development of decellularized human umbilical arteries as small-diameter vascular grafts. *Tissue Engineering Part A* 2009;15:2665-76.
12. Lin C-H, Hsia K, Ma H, Lee H, Lu J-H. In vivo performance of decellularized vascular grafts: a review article. *International journal of molecular sciences* 2018;19:2101.
13. Musil V, Sach J, Kachlik D, Patzelt M, Stingl J. Vasa vasorum: An old term with new problems. *Surgical and Radiologic Anatomy* 2018;40:1159-64.

14. Dreifaldt M, Souza DS, Loesch A, Muddle JR, Karlsson MG, Filbey D, et al. The “no-touch” harvesting technique for vein grafts in coronary artery bypass surgery preserves an intact vasa vasorum. *The Journal of thoracic and cardiovascular surgery* 2011;141:145-50.
15. Alkhalil M, Choudhury RP. Current concepts in atherosclerosis. *Indian Journal of Thoracic and Cardiovascular Surgery* 2018;34:198-205.
16. Heng JW, Yazid MD, Abdul Rahman MR, Sulaiman N. Coatings in decellularized vascular scaffolds for the establishment of a functional endothelium: A scoping review of vascular graft refinement. *Frontiers in cardiovascular medicine* 2021;8:677588.
17. Hibino N, Villalona G, Pietris N, Duncan DR, Schoffner A, Roh JD, et al. Tissue-engineered vascular grafts form neovessels that arise from regeneration of the adjacent blood vessel. *The FASEB Journal* 2011;25:2731.
18. Sánchez PF, Brey EM, Briceño JC. Endothelialization mechanisms in vascular grafts. *Journal of tissue engineering and regenerative medicine* 2018;12:2164-78.
19. Smith Jr RJ, Nasiri B, Kann J, Yergeau D, Bard JE, Swartz DD, et al. Endothelialization of arterial vascular grafts by circulating monocytes. *Nature communications* 2020;11:1622.
20. Zhang F, King MW. Immunomodulation strategies for the successful regeneration of a tissue-engineered vascular graft. *Advanced Healthcare Materials* 2022;11:2200045.
21. Graney P, Ben-Shaul S, Landau S, Bajpai A, Singh B, Eager J, et al. Macrophages of diverse phenotypes drive vascularization of engineered tissues. *Science advances* 2020;6:eaay6391.
22. Kumar A, D’Souza SS, Moskvina OV, Toh H, Wang B, Zhang J, et al. Specification and diversification of pericytes and smooth muscle cells from mesenchymoangioblasts. *Cell reports* 2017;19:1902-16.
23. Liu Y, Rayatpisheh S, Chew SY, Chan-Park MB. Impact of endothelial cells on 3D cultured smooth muscle cells in a biomimetic hydrogel. *ACS applied materials & interfaces* 2012;4:1378-87.
24. Lee JB, Park JS, Shin YM, Lee DH, Yoon JK, Kim DH, et al. Implantable vascularized liver chip for cross-validation of disease treatment with animal model. *Advanced Functional Materials* 2019;29:1900075.
25. Lee JB, Kim D-H, Yoon J-K, Park DB, Kim H-S, Shin YM, et al. Microchannel network hydrogel induced ischemic blood perfusion connection. *Nature Communications* 2020;11:615.

26. Lee S-J, Sohn Y-D, Andukuri A, Kim S, Byun J, Han JW, et al. Enhanced therapeutic and long-term dynamic vascularization effects of human pluripotent stem cell-derived endothelial cells encapsulated in a nanomatrix gel. *Circulation* 2017;136:1939-54.
27. Baek S, Yu SE, Deng YH, Lee YJ, Lee DG, Kim S, et al. Quenching Epigenetic Drug Resistance Using Antihypoxic Microparticles in Glioblastoma Patient-Derived Chips. *Advanced Healthcare Materials* 2022;11:2102226.
28. Wang X, Chan V, Corridon PR. Decellularized blood vessel development: Current state-of-the-art and future directions. *Frontiers in Bioengineering and Biotechnology* 2022;10:951644.

Abstract in Korean

무 세포 혈관 이식 그래프트의 현장 재생 촉진을 위한 인공 맥관

소구경 혈관의 병태생리 조절 패러다임은 내경, 내막의 요소가 아닌 혈관 외벽이 주요한 역할을 하는 것으로 변경되어 왔다. 혈관 외벽에서의 조절자로서의 미세혈관 (맥관)은 혈관벽의 내부와 외부 간의 상호작용 경로를 제공한다. 소구경 혈관을 제작하기 위한 수많은 접근이 있어왔지만, 지속적으로 문제가 되어온 혈전 및 혈관벽의 면역반응을 해결하기 위한 다기능적 해법으로서 인공적으로 설계 및 제작된 맥관은 제시되어 오지 못하였다. 본 연구에서는 이식 가능하며, 다양한 연구를 통하여 이식 가능성이 검증된 인공적인 맥관 구조가 미세채널 네트워크 하이드로젤을 사용하여 공학적으로 개발되었으며, 이를 동물 이식 후 기계적 특성이 보존된 탈세포 혈관의 외벽을 감싸는데 사용하였다. 토끼 모델의 소구경 혈관에서 시행한 혈관 이식 수술 후, 인공 맥관은 마이크로 채널을 통해 대식세포의 M2 양극화를 통해 세포가 없는 혈관벽에 혈관 신생 및 형성 세포 침윤 촉진을 통해 탈세포 혈관의 재세포화를 유도하였다. 이러한 기능은 혈관 평활근의 복원을 유도함으로써 혈관의 탄성을 회복하고 장기간 개통성을 유지하는데 도움을 주었다. 결과적으로, 인공 맥관은 혈관 이식시 혈관벽 재생의 효과적인 촉매 역할을 하여 성공적인 소구경 혈관의 임상적 적용의 해법을 제시하였다.

핵심되는 말: 마이크로채널 네트워크, 인공혈관, 무세포 스캐폴드, 내피세포화, 조직공학적 혈관 그래프트